R. & M. No. 3384

MINISTRY OF AVIATION

AERONAUTICAL RESEARCH COUNCIL
REPORTS AND MEMORANDA

The Development of a Nozzle for Absolute Airflow Measurement by Pitot-Static Traverse

By J. C. Ascough

LONDON: HER MAJESTY'S STATIONERY OFFICE
1964
PRICE £1 0s. 0d. NET

The Development of a Nozzle for Absolute Airflow Measurement by Pitot-Static Traverse

By J. C. Ascough

Communicated by the Deputy Controller Aircraft (Research and Development), Ministry of Aviation

*Reports and Memoranda No. 3384**
May, 1963

Summary.

A special nozzle has been made with associated ducting and instruments in order to provide an absolute measure of airflow. The equipment could form a portable self-contained assembly, enabling calibrations to be made of meters installed in test rigs.

In order to give an absolute measurement, the nozzle has been designed to generate an idealised flow amenable both to theoretical prediction and to experimental survey. Firstly, the nozzle produces a uniform velocity profile across the mainstream, which can easily be traversed for pitot and static pressure to a high order of accuracy. Secondly, the boundary layer is fairly thin in the traverse plane, thus minimising the effect of variations within it on nozzle C_D.

The discharge coefficient has been determined by traversing within the flow range from 6 to 18 lb/sec. The theoretical calculation of C_D is in good agreement with the 'traverse' results.

The uncertainty of an airflow measurement in a steady flow is estimated as $\pm 0{\cdot}17$ per cent due to known random errors. By far the biggest error is that resulting from circumferential variation of the boundary-layer profiles. It is felt that much of the error from the boundary layer could be removed with the manufacture of a new nozzle.

An extensive subsidiary experimental programme has been carried out to solve the problem of the accurate measurement of static pressure. The effect of static-hole size was found to agree with Shaw's correlation.

LIST OF CONTENTS

* Replaces N.G.T.E. Report No. R.254—A.R.C. 25 030.

LIST OF CONTENTS—*continued*

Section

LIST OF APPENDICES

Appendix

LIST OF ILLUSTRATIONS

---

1. *Introduction.*

In experimental aerodynamics it would often be an advantage to be able to measure airflow to an accuracy better than that indicated by the standard Codes. A particular requirement at the National Gas Turbine Establishment called for an absolute determination of airflow over the range from 6 to 40 lb/sec with an uncertainty of less than $\pm 0{\cdot}25$ per cent, in order to calibrate a meter installed in a test rig. To meet the requirement, it was decided to design and develop a special nozzle assembly that would generate idealised conditions in the flow. The latter would then be amenable to theoretical prediction and could also be traversed for pitot and static pressure to a high order of accuracy.

The preliminary work on the project has been reported in Ref. 1. At the time of that paper the nozzle assembly had been developed to the stage where a uniform total—and static—pressure profile could be guaranteed in the mainstream at the 7·5 in. diameter traverse plane. A boundary layer about 0·25 in. thick in the traverse plane, accounting for about an eighth of the total flow, had been partially explored. Much effort had been devoted to the problem of the accurate measurement of static pressure and, with certain qualifications, accurate values were being obtained.

During a subsequent traverse a bad local discrepancy was found in the boundary layer. The removal of a fixed pitot in the nozzle inlet eliminated the main discrepancy, but it became apparent that there remained variations in the boundary layer requiring investigation. The research into the quality of the boundary layer is described in the present report. Although the final boundary-layer quality is not ideal, a modus operandi has been reached enabling the traverses to be made for the discharge coefficient, as well as an analysis of accuracy.

For completeness, the description of the apparatus is repeated in the present report—in Section 2—and the earlier work on static pressure is summarised in Section 3. The only changes in apparatus since Ref. 1 are the new, shorter and more rigid, boundary-layer probe (Section 2.3) and the new transition device (Section 2.2). The description of the main work since Ref. 1 commences at Section 4.

2. *Description of the Calibrating Nozzle and Instruments.*

2.1. *General Lay-out.*

The calibrating nozzle with its associated ducting is shown connected to the outlet of a test rig in Fig. 1. A conical diffuser, of 6° total angle and 96 in. length, ducts the air from the 10 in. diameter rig outlet to the 20 in. diameter honeycomb and gauze sections. An alternative to the conical diffuser, for use where space is limited, is a sudden expansion from the 10 in. diameter to the 20 in. diameter, the sudden expansion being followed by a settling length 40 in. long. This alternative arrangement is satisfactory provided the high-loss gauze, causing a pressure loss of six dynamic heads, is fitted in front of the first honeycomb. A 10 in. long section immediately in front of the nozzle contains the inlet static-pressure taps, but all protrusions in the form of pitot tubes have been removed. The nozzle itself is followed by a 12 in. long instrument-mounting duct, from which the main pitot-static probe projects forward into the nozzle. A 79 in. long pipe maintains the 7·5 in. diameter of the nozzle constant for a further 10·5 diameters to the outlet valve.

2.2. *The Calibrating Nozzle.*

The nozzle, of cast Duralumin construction, is shown in Fig. 2. It is designed to fulfil the following requirements:

(*a*) To accelerate the airflow to create a suitable pressure difference.

(*b*) To give a flat velocity profile across the bulk of the throat cross-section in order to facilitate accurate measurement by a small number of traverse points.

(*c*) To have a fairly thin boundary layer at the traverse plane in order that measurement errors within the boundary layer should be of relatively small importance.

(*d*) To have a boundary layer which is consistent with time and uniform round the periphery.

Requirement (*a*) led to the choice of 7·5 in. for the throat diameter for the range of airflows from 6 to 18 lb/sec, at approximately atmospheric pressure. It was hoped to cover higher flow rates up to 40 lb/sec by increasing the pressure in the nozzle. An inlet diameter of 20 in. was chosen to give a large area-ratio contraction of 7·1/1, in order to satisfy requirement (*b*). The cubic equation $y = x^3/kD_2^2$, D_2 being the diameter of the traverse section, with $k = 20$, was taken for the profile of Section B in Fig. 2, as in the investigation by Dimmock and Parker[2]. This curve has both zero slope and zero curvature at outlet, thereby blending smoothly with the parallel section and producing only a negligible kink in the pressure distribution. The choice of $k = 20$ is a compromise, being high enough to give small values of slope and curvature yet low enough to reduce the length of Section B to minimise boundary-layer growth. With this gentle entry to the parallel section it was felt possible to put the traverse plane well forward to enjoy the benefit of a thin boundary layer.

Section A has an inverse profile equation of $Y = X^3/KD_1^2$, K being chosen to blend with equal slope into Section B.

To satisfy requirement (*d*) it is necessary to fix the point of transition from laminar to turbulent flow in the boundary layer. The original transition device, consisting of a double row of staggered pins, was removed during the earlier static-pressure investigation[1] and replaced by a hoop of 0·5 mm hypodermic tubing fixed against the nozzle wall. This second arrangement was later abandoned because of difficulty in the proper fixing of the tubing against the wall, it being felt that the tubing must form a seal with the wall, while the fillets of glue should be very small and uniform around the periphery. The tubing was replaced by a groove 0·125 in. wide × 0·025 in. deep, machined 5 in. upstream of the start of the parallel section. Another groove was added later a further 3 in. upstream.

Four bosses are positioned 90° apart in the nozzle traverse plane to take static-pressure plugs. Another four bosses 3 in. downstream provide locations for a short boundary-layer pitot probe.

2.3. *Traversing Instruments.*

In order to minimise the disturbance to the flow field in the measurement plane the traverse probes were of small diameter, while the support stem of the main probe was of aerofoil section, spanning the full diameter of the nozzle more than one diameter downstream. The length of the probes necessitated a special construction as shown in Figs. 3 and 4. Potential-flow theory for sources and sinks showed that the disturbances in static pressure in the traverse plane resulting from the main probe should be well under 0·1 per cent of the dynamic head.

Bending tests on the 10 in. long boundary-layer probe showed it to be too flexible to give the required accuracy for traversing the boundary layer. The 3 in. probe was found to be sufficiently rigid.

The tips of the boundary-layer pitots were left circular as there is recent evidence[15] that non-circular pitots are unreliable in velocity gradients. A micrometer head enabled the probes to be traversed in increments of nozzle radius of 0·001 in., an electrical signal indicating contact of the swan-neck tip with the wall.

The static holes in the main probe and the pitot hole in the boundary-layer probes were arranged to lie in the nozzle measurement plane.

Airflow total temperature was measured with N.G.T.E. type sonic suction pyrometers[3], up to three in number. These instruments have a rapid response as well as good accuracy. A 0·125 in. diameter inlet hole admits air to a 0·060 in. diameter choked nozzle across which is stretched a thermocouple wire. The sample air exhausts to suction when necessary for keeping the pyrometer nozzle choked. The smallest pyrometers, of 0·25 in. outside diameter, were too bulky to insert into the nozzle itself; instead they were traversed directly across the instrument-mounting section.

2.4. *Plugs for the Measurement of Static Pressure at the Nozzle Wall.*

It was considered to be impossible to make the static-pressure holes to the extremely high standards of precision necessary by drilling directly into the nozzle wall. Instead, the holes were made in a set of plugs which were inserted into the nozzle, flush-faced to an accuracy of about 0·0002 in.

Several types of plugs were made, the final design being shown in Fig. 5. These plugs are of brass, 1·000 in. diameter, but relieved to 0·990 in. to allow slight tilting when obtaining the flush fit. The face is radiused to 3·750 in. to suit the nozzle radius and across this face are four static holes, providing a range in diameter from 0·0116 in. to 0·0635 in. All the static holes are four diameters long; they then enlarge to twice their surface diameter before connecting with 1/16 in. inside-diameter tubing.

The manufacture of the static holes required workmanship of the highest order. Special techniques were acquired both from our own experience and by consultation with workers at the Universities of Oxford and Liverpool.

2.5. *Fixed Wall-Contact Pitots.*

Originally, two fixed pitot tubes, of 1·5 mm outside diameter, were provided to monitor the consistency of the boundary layer. The pitots were held in separate plugs and inserted in the nozzle wall on opposite ends of a diameter in the measurement plane. The tubes just touched the wall.

Subsequently, to obtain data on circumferential variation, a set of 18 fixed pitots of 0·75 mm outside diameter were fitted round the circumference of the nozzle traverse plane, with their tips in contact with the wall. The tip diameter of 0·75 mm, the same as for the new short boundary-layer probe, was the smallest size to give a satisfactory response rate—tubes of 0·5 mm outside diameter were found to be too sluggish.

2.6. *Pressure-Recording System.*

Most pressure-measuring instruments were connected *via* 3 mm inside-diameter P.V.C. tubing to water-filled vertical manometers, constructed of precision-bore glass tubes of 5 mm inside diameter. Readings of the meniscus were repeatable to about 0·01 in.

Pressures were generally measured as small differences from a reference pressure of similar magnitude. Unavoidable fluctuations in the flow then affected both pressures about equally, so that the manometer readings were steady. For pressure differences of appreciable magnitude, such as the dynamic pressure, manometers constructed from 1 in. diameter glass tubing with mirror scales were used to reduce the meniscus error.

2.7. *Instrumentation for the Indicated Mass Flow.*

The usual technique for calculating and expressing mass flow is firstly to calculate a reference or nominal mass flow on some simple basis, which is generally an idealised one-dimensional treatment, and then to obtain the true mass flow by factoring the reference or nominal mass flow by a discharge coefficient. The defect from unity in the discharge coefficient represents the proportional departure of the practical flow from, say, the idealised one-dimensional conditions assumed. As such, it is a non-dimensional quantity exhibiting only relatively small variations, so that it becomes suitable for examination either experimentally or theoretically. In the present paper the reference or nominal mass flow will be referred to as the 'indicated mass flow', so that:

$$\text{(true mass flow)} = C_D \times \text{(indicated mass flow)}.$$

The value of C_D is obtained by experimental or theoretical deduction over the required range of operation of the nozzle.

The parameters from which to calculate the indicated mass flow may be chosen on a basis of convenience—provided consistency is maintained throughout. The particular parameters used for the present nozzle are defined below, after a description of the relevant instrumentation. These parameters will be referred to as the 'indicated' values and given the subscript 'i'.

(*a*) *Indicated total pressure,* P_{Ti}.—Four 0·063 in. diameter static-pressure holes are equi-spaced round the duct circumference in a plane 5 in. upstream of the nozzle inlet. One of the holes is chosen as a reference and the absolute value of this pressure ($P_{1,\,\mathrm{ref}}$) is determined by measuring it with

respect to atmospheric pressure. The other three pressures are read independently, as differences from the reference. The mean wall static pressure at inlet, derived from the four holes, is designated $\langle P_{ws1} \rangle$. There is no need to allow for the effect of non-zero hole size in this instance because the correction is negligible at the low values of inlet dynamic pressure. The inlet dynamic pressure, h_1, is calculated from a preliminary estimate of mass flow and added to the inlet static pressure to give the indicated total pressure, P_{Ti}, thus:

$$P_{Ti} = \langle P_{ws1} \rangle + h_1. \tag{1}$$

P_{Ti} is not used directly in the formula for mass flow, but is required for the determination of the indicated dynamic pressure and the compressibility factor (*see* below).

Because of compressibility effects it is not sufficiently accurate, when calculating P_{Ti}, to make use of the standard 'velocity of approach factor':

$$\frac{1}{1-m^2} = \frac{P_{T1} - P_{s2}}{P_{s1} - P_{s2}}. \tag{2}$$

(*b*) *Indicated static pressure*, P_{si}.—Four 0·063 in. diameter static-pressure holes are equi-spaced round the circumference of the measuring plane in the nozzle throat, one hole in each of four plugs. One of the holes is chosen as a reference and the difference between this pressure ($P_{2,\,\mathrm{ref}}$), and the inlet reference pressure ($P_{1,\,\mathrm{ref}}$) is measured on a high-quality manometer (such as a 1 in. diameter, 100 in. long, vertical manometer with mirror scales). This establishes the absolute value of ($P_{2,\,\mathrm{ref}}$). The pressures from the other three holes are read independently, as differences from the measuring plane reference. The mean wall static pressure derived from the four holes is designated $\langle P_{ws2} \rangle$. A correction ($-\Delta p$), is made from Fig. 6 to allow for the effect of static-hole size in a region of high dynamic pressure and shear stress.

The data in Fig. 6 have been correlated in terms of wall shear stress, τ_w, as is usual in boundary-layer work. To convert to the more practical terms of dynamic pressure, h, the following expressions may be used:

$$\frac{\tau_w}{h} = 0{\cdot}0576 R_x^{-1/5} \tag{3}$$

$$R_x = \frac{Ux}{\nu} \tag{4}$$

and

$$U^* = \sqrt{\frac{\tau_w}{\rho}}. \tag{5}$$

The resulting corrected mean static pressure at the wall in the measuring plane is designated P_{si}, the indicated static pressure of the nozzle. Thus:

$$P_{si} = \langle P_{ws2} \rangle - \Delta p. \tag{6}$$

(*c*) *Indicated dynamic pressure*, h_i.—The indicated dynamic pressure is the difference between the indicated total pressure and the indicated static pressure. Thus:

$$h_i = P_{Ti} - P_{si}. \tag{7}$$

(*d*) *Indicated air temperature*, T_{Ti}.—Three N.G.T.E. type sonic suction pyrometers[3] are fixed with inlets 0·75 in. from the wall in the instrument-carrying section, 10 in. downstream of the measuring plane. The mean reading is designated T_{Ti}.

(*e*) *Indicated value for the compressibility factor*, β_i.—The 'compressibility factor', β, allows for the effect of compressibility on a mass-flow calculation. Its derivation is given in Appendix II, from which its indicated value is:

$$\beta_i = \left[\sqrt{\left\{\frac{\frac{1}{2}\rho U^2}{(P_T - P_s)} \times \left(\frac{T_T}{T_s}\right)\right\}}\right]_i \tag{8}$$

where all the quantities on the r.h.s. of equation (8) are those derived by the isentropic relations from P_{Ti} and P_{si}. A curve of β against P_T/P_s is shown in Fig. 7. β appears to be equivalent to the factor ϵ for nozzles in Ref. 19.

The equation for the indicated mass-flow rate {equation (II.6) of Appendix II} is:

$$W_i = A_2\beta_i \sqrt{\frac{2g}{R}} \sqrt{\frac{P_{si}h_i}{T_{Ti}}} \text{ lb/sec.} \tag{9}$$

For the present nozzle, using the gas constant for air $R = 96{\cdot}00$ ft. lbf/lb°K and the conversion factor $g = 32{\cdot}174$ pdl/lbf, equation (9) becomes:

$$W_i = 1{\cdot}3070\beta_i \sqrt{\frac{P_{si}h_i}{T_{Ti}}} \text{ lb/sec} \tag{10}$$

where the units to be used are:

P_{si} — in. of water, absolute, at 15°C

h_i — in. of water, at 15°C

T_{Ti} — °K.

3. *The Static-Pressure Problem.*

Initially it was found impossible to get any close agreement between the various measurements of static pressure. It was known[4, 5, 6] that the reading from a static hole was influenced by its geometry, in particular by its diameter and length. Even after making allowance for the geometry, however, there remained such a large variation between the readings as to necessitate an extensive subsidiary investigation into static-pressure measurement before the traversing of the nozzle could proceed.

For this investigation many different shapes and sizes of static holes were tried in the wall plugs. Experiments with static probes played a lesser part for the following reasons:

(*a*) Small probes are relatively difficult to make.

(*b*) Only one or two probes could be tested together in the nozzle, compared with large numbers of wall static holes.

(*c*) No quantitative data could be found in the literature on the performance of probes in a velocity gradient, which is said to be equivalent to a slight yaw.

(*d*) Turbulence has a significant effect[8, 9, 10, 11] not only on a static-probe reading but also on the true value of local static pressure in the boundary layer.

(*e*) The state of the private boundary layer on the surface of the probe itself would be uncertain, especially when the probe is traversed across the nozzle boundary layer. A variable transition point on the probe could play havoc with the readings of its static holes.

(*f*) Within the space limitations of a small probe the static hole can neither be rigorously proportioned nor accurately manufactured and is therefore liable to some unpredictable error. The problems existing in a pure static probe would be magnified in a small combined pitot-static instrument.

(*g*) Even if the above difficulties were overcome, it would seem unlikely that a probe could be used in a final calibration as it would be foolhardy to rely on the readings of a single instrument.

The problem of measurement of the static pressure in the nozzle was eventually solved in two stages. The first stage was to produce a number of 'identical' high-quality static holes which would give consistent readings. It can be shown[16] that if the pressure error, ΔP_ϵ, due to an imperfection of linear dimension, ϵ, were proportional to the dynamic head at distance ϵ from the wall, then

$$\frac{\Delta P_\epsilon}{h} \propto R_\epsilon{}^2 R_x{}^{-2/5} \tag{11}$$

where

$$R_\epsilon{}^2 R_x{}^{-2/5} = \left(\frac{W\epsilon}{A\mu}\right)^2 \left(\frac{Wx}{A\mu}\right)^{-2/5} \tag{12}$$

and x is the length of the turbulent boundary layer. The assumption for which equation (11) is derived may not be exact, but a similar assumption appears to give the correct form for the basic effect of hole size, so that equation (11) should indicate the correct trends. Now in the present work the mass flow per unit area, W/A, was required to be quite large, while the length, x, was deliberately kept small to give a thin boundary layer—both these factors encouraged large pressure errors by equations (11) and (12). The error $\Delta P_\epsilon/h$ is also seen to be proportional to the square of the dimension of an imperfection. The measure of the great care needed in manufacture and handling was learned in this first stage at the end of which a set of 12 identical wall-plug static holes, of comparatively large size, 0·063 inch diameter, were successfully made to the necessary precision to give consistent readings. In a test at a dynamic head of about $h = 78$ inches of water, the scatter of the readings from the 12 high-quality static holes was $\pm 0{\cdot}18$ per cent of h about the mean. (The standard deviation was $\sigma P_s/h = 0{\cdot}00088$ or 0·088 per cent while the standard deviation of the mean pressure was $\sigma(\bar{P}_s)/h = 0{\cdot}00088/\sqrt{12} = 0{\cdot}00025$ or 0·025 per cent.)

Having learned how to measure the static pressure consistently with holes of one size, the next stage was to check the effect of hole size. Four plugs made to the scheme of Fig. 5, containing a range of hole size from 0·011 in. to 0·063 in., provided data on the effect of hole diameter. During the investigation it was decided to remove the original boundary-layer transition fence, consisting of a staggered double row of pins, 0·036 in. diameter × 0·040 in. high, which, it was suspected, had been the cause of some of the scatter in the static-pressure readings. It was replaced by a continuous hoop of 0·5 mm hypodermic tubing glued to the nozzle wall. This arrangement did reduce the scatter in the static-pressure readings, but the glued attachment was not completely reliable and so the hoop was in turn replaced by two-dimensional grooves machined in the nozzle wall (Section 4.2.3).

The results obtained from the holes of different size are shown in Fig. 6 in non-dimensional form, correlated on a basis of shear-stress Reynolds number. The data agree so well with Shaw[4] that we have drawn his curve through our points. However, there is still some controversy about the final extrapolation to zero for $R_U{}^*{}_{,d}$ less than 50—*see* Lester[17]. Further investigation of this issue is

under review—the proposal being to take as a fundamental pressure the reading of a flush-diaphragm transducer—but this is beyond the scope of the present work. Meanwhile we accept the correlation of Fig. 6, bearing in mind that should any further systematic error in static-pressure measurement be proved, then this will not affect the numerical value of the discharge coefficient for the nozzle (*see* Appendix IV, Section 1.1) but will affect the absolute measurement of air mass-flow rate. The scatter of the points about the curve in Fig. 6 is partly random and partly due to a very slight disagreement between Shaw's curve and the results of the present experiment. The standard deviation of the points about the curve is $\sigma(\Delta p/T_w) = 0{\cdot}170$. The equivalent typical value in terms of $\Delta p/h$ is approximately $\sigma(\Delta p/h) = 0{\cdot}000595$. (These statistics will be required later in the analysis of accuracy.) When examining the correlation it should be remembered that in Fig. 6 each group of points represented by a particular symbol can, as a group, be placed arbitrarily on the ordinate scale (in the usual way for this type of experiment) as described in Refs. 1 and 5, since the true reading for zero hole size is initially unknown.

In Fig. 6 some of the data were obtained with the nozzle inhaling from atmosphere and discharging to suction, while the remaining data were obtained with the nozzle receiving air from the plant compressors through the rig and discharging unthrottled to atmosphere. For a consistent correlation it was found—despite the presence of the settling length—that there must not be any partly open valve near the inlet to the nozzle. In fact, one test of a good installation is to take the readings from all the static holes and check that the data agree with Fig. 6. Similarly, it has not been found acceptable so far to operate the nozzle at high pressure—by throttling the pipe at the valve downstream of the nozzle. Such operation has produced a large scatter in the static-pressure readings, apparently because of pressure pulsations. Consequently operation at high pressure, which would have raised the upper limit to the range of airflow, has been postponed. It is hoped to investigate this problem at a later date.

The largest holes are least prone to the effects of blemishes and dirt, even though they suffer the greatest effect of size. Consequently the recommended method for determining the wall static pressure is to read the four 0·063 in. wall statics separately and then apply the correction for hole size to the mean reading, using Shaw's curve as reproduced in Fig. 6.

Within the boundary layer at the measuring section we have no reliable probe measurements of static pressure, particularly because of reasons (*c*), (*d*) and (*e*) above. However, the static-pressure profile has been calculated using Klebanoff's data[10] on turbulent velocities and the effect on measured mean velocities deduced by the method of Dutton[11]. The result was found to be that, although the static pressure within the boundary layer differs from the value at the wall by as much as 0·3 per cent of the mainstream dynamic pressure, this difference only negligibly reduces the discharge coefficient—by 0·00028. Hence the wall static pressure is assumed to hold throughout the boundary layer.

Another calculation has shown that the static-pressure difference between the two sides of the boundary layer is negligible, even though there is an appreciable variation within it. Consequently the static reading of the main traverse probe at the edge of the mainstream can be corrected to be equal to the true wall static. The corrected traverse of the probe will then measure the true static pressure across the mainstream. Thus the traverse probe in the mainstream is only relied upon for relative measurement.

The above appears to be the only practicable method of obtaining accurately the distribution of static pressure across the whole traverse plane; ideally the distribution would be measured directly.

4. *The Investigation of the Boundary Layer.*

4.1. *Preliminary Circumferential Traverse with the* 10 *in. Long Probe.*

In an early arrangement of the instrumentation, four small pitot tubes were fitted in the nozzle inlet section to measure inlet total pressure. With this arrangement it was suspected that a curiously low value of C_D obtained in one particular experiment was due to a boundary-layer traverse being carried out accidentally in the wake behind one of the inlet pitots, the wake perhaps having induced premature transition. A circumferential traverse was therefore made by rotating the instrument section behind the nozzle so that the 10 in. long boundary-layer probe was swept round the circumference, readings being taken at wall-contact ($y = 0{\cdot}010$ in.) and also at $y = 0{\cdot}110$ in.

The results are shown in Fig. 8. The dip at $\theta = 40°$ is of about the right magnitude to explain the low C_D and the suspected inlet pitot was, on this occasion, at $\theta = 45°$. The implied wander of 5° between the pitot and the dip in the profile could perhaps be due to some error in the setting up and measurement of θ and/or the possibility of slight swirl, e.g. $\frac{1}{2}°$ of swirl would entirely explain the discrepancy. The results of Fig. 8 are not quantitatively reliable as later tests showed the 10 in. probe to be too flexible.

4.2. *Attempted Improvements.*

4.2.1. *Inlet arrangement.*—All of the inlet pitots were removed and their function, the measurement of the inlet pressure, transferred to four inlet wall static-pressure taps. The change caused extra computational labour since the standard incompressible 'velocity of approach factor', $(1-m^2)$, was found to be not accurate enough in estimating the effect of inlet dynamic pressure.

The grid supporting the gauze nearest to the nozzle inlet was also removed, after checking that the gauze was strong enough to support itself against the drag of the nozzle inlet airflow. The grids on the other gauzes were chamfered at their trailing edge.

4.2.2. *Surface quality of the nozzle wall.*—The first machining of the Duralumin casting for the nozzle revealed a large number of small blow holes breaking the surface. Most of the holes in the parallel throat section and near approach to it were filled before the final machining of the nozzle profile. But there remained some holes which were particularly undesirable in the near approaches to the parallel throat, where they could cause premature transition of the laminar boundary layer. An attempt to fill in these remaining holes was not successful and had to be abandoned. It would probably be better to make future nozzles by some other technique, such as electro-deposition or spinning, to avoid blow holes.

4.2.3. *Transition devices.*—A hoop of 0·5 mm hypodermic tubing had been fitted to the nozzle wall 4·5 in. upstream of the start of the parallel section to fix boundary-layer transition. As mentioned earlier this had replaced the arrangement of a double row of pins. Unfortunately, no satisfactory method of fixing the hoop against the wall could be discovered—only the slightest trace of adhesive seemed permissible—with the result that the hoop was liable to lift away from the wall.

Since the whole object of the transition device is to ensure a reliable boundary layer, it follows that the device itself must be impeccable. Therefore, it was decided to provide a really permanent device in the form of a groove, 0·125 in. across × 0·025 in. deep, machined round the nozzle circumference 5 in. upstream of the start of the parallel section. Subsequently, another groove was machined a further 3 in. upstream, with the object of forestalling premature transition which, it

was thought, might be occurring at some of the imperfections in the nozzle surface. Ref. 11 indicates that the critical Reynolds number for the grooves should be equivalent to a nozzle mass flow of about 6 lb/sec for the rear groove and 7 lb/sec for the front groove.

Even the groove arrangement, in its present form, is not perfect as the blow holes give it an irregular edge. In any new build of nozzle, a more satisfactory transition device could be similar to the arrangement of Preston[21] with a projecting ring clamped in a spigoted flange specially provided in the transition plane.

With the improved arrangements at inlet, and with the two grooves to provide transition, circumferential traverses with the 10 in. long probe showed that the dip at $\theta = 40°$ in Fig. 8 had disappeared but that the general variability was only a little better. The remainder of Section 4 describes the much more detailed investigation which was found necessary to assess this and other sources of error in the boundary layer.

4.3. *An Experiment with the Wall-Contact Pitots.*

Two tests were carried out with a batch of 18 wall-contact pitots distributed around the circumference of the nozzle traverse plane. The results are shown in Fig. 9.

Between Test A and Test B, three pairs of pitots were interchanged, while six pitots were moved and reset leaving six unchanged, as indicated in the figure. In the course of each individual test, six manometer connections were interchanged.

In the lower part of the figure, the differences between the two sets of values of $(P_T - P_{si})/h_i$ have been analysed according to causes; the phrase 'difference due to tests' refers to the difference occurring in a reading between Tests A and B when no apparent change had been made in the conditions. The results are summarised in the following table:

TABLE 1

Cause of difference	Mean difference
Manometers	negligible
Tests	0·004
Tests + resets	0·007
Pitots + tests + resets	0·021
θ + tests + resets	0·027

It is obvious that important differences exist between individual pitots (surprisingly), and also between circumferential angles. An allowance must therefore be made for these.

4.4. *Further Comparison with Wall-Contact Pitots.*

The large differences between the pitots of Section 4.3 raised doubts about the quality of manufacture and fitting. Subsequent examination of the pitots under the microscope suggested, in particular, that near the tips the diameters were slightly reduced. Hence a second batch was made, taking extra special care. The faces were lapped flat with diamond paste and the true diameters of the pitot tips were preserved. When fitting the pitots for wall-contact, care was taken not to distort the surfaces.

The results are shown as Test C in Fig. 10, to be compared with Tests A and B reproduced from Fig. 9.

A rigorous statistical t-test showed that the difference between the mean of Test A and the mean of Test C was highly significant. This would be explained physically by the full tip diameter of the second batch (no metal removed in manufacture) causing the tip centres to be farther from the wall and therefore to read higher. However, a statistical variance ratio F-test between the Tests A and C was not significant. This implies that the general scatter about the mean due to circumferential angle and individual foibles of the pitots was the same for both batches.

Test D was a repeat of Test C with improved rig operating conditions, the airflow being controlled by a valve very much farther upstream of the test rig. A statistical t-test and F-test showed no significant differences between Tests C and D. This result, showing the insensitivity of the pitots to rig operating conditions, is in marked contrast to the behaviour of the wall static-pressure tappings, which were badly affected by rig conditions similar to Test C.

At the bottom of Fig. 10 are the readings of the new 3 in. long boundary-layer pitot at wall-contact at the four possible circumferential stations. This probe has the same tip diameter of 0·75 mm as the 18 fixed pitots. It may be seen that the results of Tests C and D are not inconsistent with the results of the boundary-layer probe, in that, as might be expected, the means are comparable and the scatter is of the same order of magnitude. Consequently, in subsequent analyses the combined standard deviation, $\sigma = 0{\cdot}0145$, from Tests C and D on the 18 pitots, will be used as a measure of:

(*a*) Differences in a larger sample of circumferential wall-contact points than can be sampled by the boundary-layer probe.

(*b*) Differences between a large number of individual pitots of which the boundary-layer pitot is a single example.

4.5. *Circumferential Variation of Dynamic Pressure in the Boundary-Layer Traverses with a 3 in. Long Probe.*

Traverses across the boundary layer were made at four circumferential points with the 3 in. long probe. At each chosen value of y (the radial distance in from the wall) the total circumferential range, from minimum to maximum, of $(P_T - P_{si})/h_i$, defined as $\Delta[(P_T - P_{si})/h_i]$, was noted and is plotted in Fig. 11. It can be seen that the value of Δ at wall-contact is slightly greater than the mean value throughout the boundary layer. Thus, if we assert that a wall-contact measurement of variance is typical of the whole boundary layer we shall obtain a slightly pessimistic estimate of accuracy. This will be our justification for taking the wall-contact value of overall standard deviation (*see* Section 4.4), i.e. $\sigma = 0{\cdot}0145$ for $h_i \simeq 50$ in. of water, and applying it throughout the boundary layer.

4.6. *Effect of Pitot-Tube Size.*

The traverse results given by pitot probes of three different tip diameters are shown in Fig. 12 for $h_i \simeq 50$ in. of water. Mean results for two different probes of the same size are given for each of the 0·75 mm and 1·5 mm tips. The result for the 3 mm tip is that of a single probe.

The convention is to regard the reading of a pitot of finite size as a value appropriate to an effective distance of the tip centre from the wall, y_e, which is greater than the actual distance, y_a, by the displacement ϵ. Curves of ϵ/D, where D is the tube outside diameter, deduced from the 0·75 mm and 1·5 mm pitots of Fig. 12, and again as deduced from the 0·75 mm and 3 mm pitots of Fig. 12, are given in Fig. 13.

The approximate mean value of $e/D = 0{\cdot}15$ agrees with the best compromise from the literature[13, 14, 15]. We will assert that the true value is $0{\cdot}15 \pm 0{\cdot}05$, to be used in the analysis of accuracy.

5. *The Final Traverses.*

5.1. *The Boundary-Layer Traverses.*

Pitot traverses were made with the 3 in. long probe of Fig. 4 at the four circumferential stations: 3, 6, 9 and 12 o'clock, for values of the indicated dynamic pressure of about 20, 50 and 120 in. of water. As an example, the set of results taken at $h \simeq 50$ in. of water are shown in Fig. 14.

As explained in Section 3, the corrected average wall static is taken for the static pressure within the boundary layer.

5.2. *The Mainstream Traverses.*

The mainstream was traversed with the pitot-static probe of Fig. 3. The pitot and static readings were taken independently, backed off against their respective reference pressures on the manometers. An example of a set of traverses is shown in Fig. 15.

To illustrate the uniformity of the static pressure in the mainstream the probe readings are plotted as differences from the readings at the edge of the mainstream. The absolute value of the static-pressure profile is obtained by adding the corrected average wall static to this plot, since it is shown in Section 3 that the static pressure is equal on either side of the boundary layer.

5.3. *Temperature Traverses.*

The tests had been carried out with air near to room temperature, i.e. between 15°C and 30°C. Early six-point traverses across the instrument duct with the sonic suction pyrometer showed a mean range of temperature only 0·4°C from duct axis to wall, for $h_i \simeq 50$ in. of water. The corresponding standard deviation from quality control tables was $\sigma(T) = 0{\cdot}158$°C, while the standard deviation of the traverse mean was $\sigma(\text{traverse mean } T) = \sigma(T)/\sqrt{6} = 0{\cdot}0646$°C. Consequently the inlet of the pyrometer was fixed at 0·75 in. from the wall, a position which for the present set of tests gave the traverse mean reading directly.

6. *The Discharge Coefficients.*

6.1. *Traverse Results.*

A calculation of a discharge coefficient was made based on each boundary-layer traverse together with an associated mainstream traverse, the latter being, for convenience, that taken in the same test run as the boundary-layer traverse but across the other diameter of the measuring section. The corresponding temperature traverse was that for the opposite side of the duct. In this way a set of traverses taken at approximately the same time and at the same operating condition was used for the calculation. The results were integrated by the method of Appendix II by desk machine to give the values shown in Fig. 16, where C_D is plotted against air mass-flow rate or nozzle Reynolds number. The scatter of the individual points on the graph largely reflects the circumferential variation of the boundary-layer profile (*see* Table 2 in Appendix IV, Section 2.1). The curve of the mean traverse C_D gives the recommended best value.

6.2. *Theoretical Results, and Comparison between Theory and Experiment.*

The three curves of theoretical C_D shown in Fig. 16, calculated by the method of Appendix III, are based on the following assumptions:

Curve (*a*) Laminar boundary layer right up to the nozzle traverse plane.

Curve (*b*) Laminar boundary layer up to the first transition groove and turbulent boundary layer thereafter, with no allowance for losses at the two grooves.

Curve (*c*) As Curve (*b*), but corrected for compressibility for the Mach numbers (from $M = 0{\cdot}25$ to $M = 0{\cdot}6$) obtaining during the traverse tests.

It may be noted that if the flow were at a higher pressure, and therefore at a higher density, for the same values of mass-flow rate and Reynolds number, then the divergence of Curve (*c*) from Curve (*b*) would be less. If the fluid were incompressible, e.g. water, Curve (*b*) would apply uniquely as a curve of discharge coefficient against Reynolds number. The critical mass flows, W_{crit}, indicated in Fig. 16, are those below which the boundary layer is likely to remain laminar; they have been calculated from the critical Reynolds number for the transition grooves of 1200, based on groove width and mainstream velocity[12].

It appears that the curve of mean traverse C_D is in quite good agreement with theoretical Curve (*c*). An allowance for losses at the grooves could make the agreement even closer.

7. *Discussion.*

7.1. *The Philosophy of the Method for Absolute Airflow Measurement.*

The claim that a measurement is absolute requires careful examination when the method employed is inferential in character. The case is less obvious than for, say, the measurement of fluid flow by positive displacement to or from a container.

In Appendix II the equation (II.4) for mass-flow rate is developed from the pure, self-evident, but immeasurable form:

$$\delta W = \rho u \delta A$$

to an equation (II.14) which is amenable to measurement:

$$\delta W = \beta \sqrt{\frac{2g}{R}} \sqrt{\left\{\frac{P_s(P_T - P_s)}{T_T}\right\}} \delta A$$

where, as equation (II.13):

$$\beta = \sqrt{\left\{\frac{\frac{1}{2}\rho u^2}{(P_T - P_s)} \left(\frac{T_T}{T_S}\right)\right\}}$$

The density and velocity factors in equation (II.4) quoted above have been replaced by means of equation (II.8):

$$\rho = \frac{P_s}{RT_s}$$

and equation (II.5):

$$(P_T - P_s) = \tfrac{1}{2}\rho u^2 \alpha$$

where α is a function of Mach number, nearly equal to unity.

If the total and static pressure and total temperature in equation (II.4) can be measured absolutely, then there seems little doubt that an absolute measurement of mass flow will result.

In the present investigation it is believed that all known effects which could influence the experimental readings have been taken into account. The effects considered include:

(*a*) Effects of hole size and operating conditions on static-pressure measurement.

(*b*) Effect of pitot-tube shape and size in the boundary layer.

(*c*) Interference from the traverse probes.

(*d*) Theoretical variation of static pressure in the boundary layer (it was deduced that experimental measurement was impossible in this region).

The errors remaining are those due to the limited sampling provided by the traverses, and those due to imperfections in instrumentation. The procedure followed in meeting the first source of error has been to make the flow as uniform as possible, and then to assess the residual sampling errors from the scatter in the results. The random errors due to imperfections in the instrumentation have been assessed from the scatter of results taken from several instruments. The assessment is made in Appendix IV.

As a guard against the possibility of any unforeseen systematic effect or error being present in the measurements, use was made, wherever possible, of check criteria. For example the traverse pitot readings in the mainstream were checked against the inlet total pressure, while the readings of the boundary-layer pitot at wall-contact were checked against the fixed wall-contact pitots. The bending of the boundary-layer pitot was studied carefully (*see* Appendix IV, Section 1.5). The effect of pitot-tube size in the boundary layer was observed to agree sufficiently well with the results of other workers, while the effect of wall static-hole size and operating conditions was found to agree with Shaw (but *see* Section 7.3 below).

7.2. *Accuracy of the System and Possible Improvements.*

It is shown in the analysis in Appendix IV that the uncertainty due to the random errors in a mass-flow measurement is about $\pm 0{\cdot}17$ per cent, provided the flow is steady. It is felt that one element of error, that due to circumferential variations in the boundary layer, could be reduced with the manufacture of a new nozzle, possibly by electro-deposition or spinning, thus avoiding casting blow holes. In this way the uncertainty of $\pm 0{\cdot}17$ per cent might be reduced to about $\pm 0{\cdot}11$ per cent.

It might also be more satisfactory to use the transition arrangement of Preston[21] where a projecting ring is clamped between two spigoted flanges specially provided in the transition plane.

7.3. *Systematic Error in the Measurement of Static Pressure.*

To all appearances, Shaw's curve fits our data in Fig. 6 very well. There is, however (as stated in Section 3) still some controversy about the final extrapolation to zero for $R_U{}^*{}_{,d}$ less than 50 for example. Indeed, Lester[17] suggests that the intercept should be as much as 3 units of $\Delta p/\tau_w$ less than Shaw's value. This would be equivalent to an error of about $0{\cdot}5$ per cent of mass flow. Some workers, e.g. Thwaites[18], question the philosophy of an open hole of any size for an absolute measurement of static pressure, preferring if possible a flush-diaphragm type of instrument.

The problem is under review and the issue may be settled soon. When the final answer is found we must be prepared to adjust accordingly the corrections applied to the indicated instrumentation, although the numerical value of the discharge coefficient will remain unchanged (*see* Appendix IV, Section 1.1).

8. *Conclusions.*

(1) The present airflow calibrating nozzle provides an absolute measurement of airflow over the range from 6 to 18 lb/sec. The 95 per cent confidence limit is $\pm 0 \cdot 17$ per cent when taking into account random errors known to exist in a steady flow.

(2) By far the biggest component of random error results from the boundary-layer profiles. The error arises mainly from (*a*) circumferential variation of the boundary-layer profile and (*b*) differences between individual pitots. It is felt that component (*a*) could be improved with a new build of nozzle, and that the random error could be reduced from $\pm 0 \cdot 17$ per cent to perhaps $\pm 0 \cdot 11$ per cent.

(3) A theoretical calculation of C_D, assuming a laminar boundary layer up to the first transition groove and a turbulent boundary layer thereafter, is in good agreement with the C_D obtained from the traverses.

(4) An extensive subsidiary experimental programme has been carried out in an attempt to solve the problem of the accurate measurement of static pressure. The effect of static-hole size was found to agree with Shaw's correlation.

(5) Apparently because of the disturbing effects of pressure pulsations, the nozzle cannot at present be operated satisfactorily at high pressure. A check of the acceptability of an installation is to measure the scatter about the hole-size correlation curve of the readings of the static-pressure tappings in the nozzle.

Acknowledgement.

The author wishes to acknowledge the special interest and co-operation of Dr. B. S. Stratford who advised on most aspects of the work during frequent discussions.

REFERENCES

No.	Author(s)	Title, etc.
1	B. S. Stratford and J. C. Ascough	A recent attempt at accurate airflow measurement by pitot-static traverse. N.E.L. Symposium on flow measurement in closed conduits. Paper A-6. 1960.
2	N. A. Dimmock and R. Parker ..	A multi-hole orifice plate for airflow measurement and its calibration by traversing a nozzle. A.R.C. 19 876. September, 1957.
3	C. G. Stanworth	Suction pyrometers. I.Mech.E. Symposium on some developments in techniques for temperature measurement. Paper 1, Session 1. 1962.
4	R. Shaw	The influence of hole dimensions on static pressure measurement. *J. Fluid Mech.*, Vol. 7, Part 4, pp. 550 to 564. April, 1960.
5	R. E. Rayle	An investigation of the influence of orifice geometry on static pressure measurements. S.M. Thesis, Mass. Inst. Tech., Dept. Mech. Eng. 1949.
6	A. K. Ray	On the effect of orifice size on static pressure reading at different Reynolds numbers. *Ingenieur-Archiv.*, Vol. 24, No. 3, p. 171. 1956. Translated by Sylvia W. Skan, Aerodynamic Division, N.P.L. A.R.C. 18 829. November, 1956.
7	R. C. Dean	Aerodynamic measurements. Mass. Inst. Tech. 1953.
8	S. Goldstein	A note on the measurement of total head and static pressure in a turbulent stream. *Proc. Roy. Soc.* A., Vol. 155, pp. 570 to 575. July, 1936.
9	A. Fage	On the static pressure in fully developed turbulent flow. *Proc. Roy. Soc.* A., Vol. 155, pp. 575 to 596. July, 1936.
10	P. S. Klebanoff	Characteristics of turbulence in a boundary layer with zero pressure gradient. N.A.C.A. Report 1247. 1955.
11	R. A. Dutton	The velocity distribution in a turbulent boundary layer on a flat plate. A.R.C. C.P.453. October, 1957.
12	J. B. Peterson and E. A. Horton ..	An investigation of the effect of a highly favourable pressure gradient on boundary-layer transition as caused by various types of roughness on a 10 ft diameter hemisphere at subsonic speeds. N.A.S.A. Memo. 2-8-59L. TIL/6321. April, 1959.
13	A. D. Young and J. N. Maas ..	The behaviour of a pitot tube in a transverse total-pressure gradient. A.R.C. R. & M. 1770. September, 1936.

REFERENCES—*continued*

No.	*Author(s)*	*Title, etc.*
14	F. A. MacMillan	Experiments on pitot tubes in shear flow. A.R.C. R. & M. 3028. February, 1956.
15	S. Dhawan and B. R. Vasudeva ..	The pitot tube displacement effect in boundary layers. *J. Aero. Soc.*, India, Vol. 11, No. 1. 1959.
16	B. S. Stratford	Unpublished work at the M.o.A. 1963.
17	W. G. S. Lester	Some problems of fluid flow at low speeds. University of Oxford Thesis. 1960.
18	B. Thwaites	Outline of a proposal for experiments on static pressure. A.R.C. 22 034. June, 1960.
19	British Standards Institution ..	Flow measurement. B.S.1042:1943. October, 1951.
20	B. S. Stratford	The prediction of separation of the turbulent boundary layer. *J. Fluid Mech.*, Vol. 5, Part 1, pp. 1 to 16. January, 1959.
21	J. H. Preston	The minimum Reynolds number for a turbulent boundary layer and the selection of a transition device. *J. Fluid Mech.*, Vol. 3, Part 4. pp. 373 to 384. January, 1958.
22	B. S. Stratford and G. S. Beavers	The calculation of the compressible turbulent boundary layer in an arbitrary pressure gradient—a correlation of certain previous methods. A.R.C. R. & M. 3207. September, 1959.

APPENDIX I

Notation

Symbol	*Title*	*Consistent units (ft, lb, sec)*	*Working units*
A	actual cross-section flow area	ft^2	in^2
A'	effective cross-section flow area	ft^2	in^2
C_D	discharge coefficient $= W_{\text{true}}/W_i$	N.D.	
d	diameter of static holes	ft	in.
D	either (a) inside diameter of the nozzle or (b) outside diameter of pitot tube	ft	in. or mm
$E(f)$	random error of the parameter f, at 95 per cent confidence level $= t \times \sigma(f)$	as (f)	
f	a general parameter	as appropriate	
Δf	range of the parameter f	as appropriate	
F	Fisher's variance ratio $= \sigma_a^2/\sigma_b^2$	N.D.	
g	conversion factor $= 32{\cdot}174$	poundals/lbf	poundals/lbf
h	dynamic pressure $\doteq \frac{1}{2}\rho U^2$ $= (P_T - P_s)$ for incompressible flow	lbf/ft^2	in. of water
h_i	indicated dynamic pressure $= P_{Ti} - P_{si}$	lbf/ft^2	in. of water
h_1	inlet dynamic pressure	lbf/ft^2	in. of water
k	constant in nozzle profile equation	N.D.	
K	constant in nozzle profile equation	N.D.	
l	general length dimension	ft	
m	nozzle contraction area ratio $= A_2/A_1$	N.D.	
M	Mach number	N.D.	
n	number in sample	N.D.	
P	pressure	lbf/ft^2	in. of water
$P_{s,\text{edge}}$	probe P_s at edge of mainstream, i.e. at 3·5 in. traverse radius	lbf/ft^2	in. of water
P_{si}	indicated static pressure $= \langle P_{ws2} \rangle - \Delta p$	lbf/ft^2	in. of water

Symbol	*Title*	*Consistent units (ft, lb, sec)*	*Working units*
P_{Ti}	indicated total pressure $= \langle P_{ws1} \rangle + h_1$	lbf/ft²	in. of water
$\langle P_{ws1} \rangle$	mean wall static pressure in inlet plane	lbf/ft²	in. of water
$\langle P_{ws2} \rangle$	mean wall static pressure in nozzle measuring plane	lbf/ft²	in. of water
Δp	excess reading of static pressure due to hole size	lbf/ft²	in. of water
q	dynamic pressure near gauzes	lbf/ft²	in. of water
$R_{u,l}$	Reynolds number $= \frac{\rho u l}{\mu}$	N.D.	
R_2	nozzle throat radius	ft	in.
R	gas constant $= \frac{P_s}{\rho T_s}$	ft²/sec².°K	
t	'Students' t-factor	N.D.	
T	temperature	°K	°C
u	general velocity	ft/sec	ft/sec
U	mainstream velocity	ft/sec	ft/sec
U^*	shear-stress velocity $= \sqrt{\frac{\tau_w}{\rho}}$	ft/sec	ft/sec
W	mass-flow rate	lb/sec	lb/sec
x	either (*a*) nozzle profile co-ordinate or (*b*) length of boundary layer	ft	in.
X	either (*a*) nozzle profile co-ordinate or (*b*) equivalent length of boundary layer	ft	in.
y	either (*a*) nozzle profile co-ordinate or (*b*) distance in boundary layer from wall	ft	in.
Y	nozzle profile co-ordinate	ft	in.
β	compressibility factor $= \sqrt{\left\{\frac{\frac{1}{2}\rho U^2}{(P_T - P_s)} \times \frac{T_T}{T_s}\right\}}$	N.D.	
β_i	the value corresponding to the indicated pressure ratio, P_{Ti}/P_{si}		

Symbol	*Title*	*Consistent units (ft, lb, sec)*	*Working units*
δ^*	boundary-layer displacement thickness	ft	in.
ϵ	displacement of effective centre of pitot tube	ft	in.
θ	angle round the nozzle		degree
μ	viscosity	lb/ft. sec	lb/ft. sec
ν	kinematic viscosity $= \mu/\rho$	ft^2/sec	ft^2/sec
ρ	density	lb/ft^3	lb/ft^3
$\sigma(f)$	standard deviation of f	as f	
$\Sigma(f)$	summation of the parameters, f	as f	
τ_w	wall shear stress	lbf/ft^2	in. of water

Suffices

a	actual
e	effective
i	indicated
ref	reference
true	true
s	static
T	total (stagnation)
t	transition
w	wall
1	nozzle inlet
2	nozzle throat traverse plane

APPENDIX II

The Calculation of the Discharge Coefficient from Traverse Results

The discharge coefficient is defined as the ratio of the true mass-flow rate through the nozzle to the indicated flow rate. Thus:

$$C_D = \frac{W_{\text{true}}}{W_i}. \tag{II.1}$$

The basis of the present method of calculation is the determination of the local values of the true mass-flow rate from the traverses for pitot and static pressure and temperature. An integration then yields the total true flow rate:

$$W_{\text{true}} = \int \delta W \tag{II.2}$$

which could be divided by W_i to give C_D according to equation (II.1). In practice it is an advantage to make the calculation non-dimensional throughout:

$$C_D = \int \frac{\delta W}{W_i}. \tag{II.3}$$

A convenient method of calculation was found to be as follows. We have:

$$\delta W = \rho u \delta A. \tag{II.4}$$

Let the parameter, α, be defined by:

$$(P_T - P_s) = \tfrac{1}{2}\rho u^2 \alpha. \tag{II.5}$$

Then

$$u = \sqrt{\frac{2(P_T - P_s)}{\alpha\rho}}. \tag{II.6}$$

Therefore from equations (II.4) and (II.6):

$$\delta W = \sqrt{\frac{2\rho(P_T - P_s)}{\alpha}}\,\delta A. \tag{II.7}$$

But

$$\rho = \frac{P_s}{RT_s} \tag{II.8}$$

and hence, substituting for ρ in equation (II.7) from equation (II.8):

$$\begin{aligned}\delta W &= \sqrt{\frac{2P_s(P_T - P_s)}{\alpha R T_s}}\,\delta A \\ &= \sqrt{\frac{2}{\alpha R}}\sqrt{\frac{P_s(P_T - P_s)}{T_s}}\,\delta A.\end{aligned} \tag{II.9}$$

Since it is the total temperature, rather than the static, which is measured, equation (II.9) is re-arranged as:

$$\delta W = \sqrt{\left(\frac{2}{\alpha R}\frac{T_T}{T_s}\right)}\sqrt{\frac{P_s(P_T - P_s)}{T_T}}\,\delta A. \tag{II.10}$$

In the above treatment fundamental units are assumed; in particular the pressures would be expressed in pdl/ft². To convert from poundals to lbf we would introduce the standard factor, $g = 32{\cdot}174$ pdl/lbf. Thus:

$$\delta W = \sqrt{\frac{2g}{R}} \sqrt{\left(\frac{1}{\alpha}\frac{T_T}{T_s}\right)} \sqrt{\frac{P_s(P_T - P_s)}{T_T}}\, \delta A . \tag{II.11}$$

The second factor in equation (II.11) is given the symbol β, thus:

$$\beta = \sqrt{\left(\frac{1}{\alpha}\frac{T_T}{T_s}\right)} \tag{II.12}$$

$$= \sqrt{\left(\frac{\frac{1}{2}\rho u^2}{(P_T - P_s)}\frac{T_T}{T_s}\right)} . \tag{II.13}$$

β is a function of Mach number and is plotted against pressure ratio in Fig. 7. β is not very sensitive to P_T/P_s. Any percentage error in P_T/P_s would be diminished about 29 times in β.

Hence, we have from equations (II.11) and (II.12):

$$\delta W = \beta \sqrt{\frac{2g}{R}} \sqrt{\frac{P_s(P_T - P_s)}{T_T}}\, \delta A . \tag{II.14}$$

The 'indicated mass flow', to which the discharge coefficient is related, is defined arbitrarily, as discussed in Section 2.7. The definition for the present nozzle is obtained by the insertion of the 'indicated values' as given by the fixed instrumentation—see Section 2.7—in equation (II.14) and integrating across the nozzle flow cross-section:

$$W_i = \beta_i \sqrt{\frac{2g}{R}} \sqrt{\frac{P_{si} h_i}{T_{Ti}}} \int \delta A \tag{II.15}$$

$$= A_2 \beta_i \sqrt{\frac{2g}{R}} \sqrt{\frac{P_{si} h_i}{T_{Ti}}} . \tag{II.16}$$

Therefore from equations (II.3), (II.14) and (II.16):

$$C_D = \int \frac{\beta}{\beta_i} \sqrt{\left(\frac{P_s}{P_{si}}\frac{(P_T - P_s)}{h_i}\frac{T_{Ti}}{T_T}\frac{\delta A}{A_2}\right)} . \tag{II.17}$$

Expressing the area ratio in terms of radius:

$$\frac{\delta A}{A_2} = \frac{2r\delta r}{R_2^2} . \tag{II.18}$$

Therefore from equations (II.17) and (II.18):

$$C_D = \frac{2}{R_2^2 \beta_i} \int \beta \sqrt{\left(\frac{P_s}{P_{si}}\frac{(P_T - P_s)}{h_i}\frac{T_{Ti}}{T_T}\right)}\, r\, \delta r . \tag{II.19}$$

Now it has been found experimentally that, in the present tests, the temperature sampled at the $\frac{3}{4}$ duct radius position (10 in. downstream of the traverse plane) gave the traverse mean temperature directly, and the variations across the traverse are extremely small (Section 5.3). This same temperature reading is also taken for the 'indicated' value. Consequently in the present tests it is permissible to eliminate the temperature ratio in equation (II.19).

In practice it is convenient to plot the non-dimensional ratios P_s/P_{st} and $(P_T-P_s)/h_i$ on graphs to check the progress of the traverses, but the actual integration of equation (II.19) has been carried out by desk machine. The increments in radius can be as large as 0·5 in. in the mainstream, because of the uniform profiles there, but in the boundary layer the increments used are much smaller, viz., $\delta r = 0{\cdot}020$ in., in the interests of accuracy.

If it were desired to use the slide rule (with its limited intrinsic accuracy) to calculate C_D then a useful re-arrangement of equation (II.19) is as follows:

$$C_D = 1 - \left\{ \int \left[1 - \frac{\beta}{\beta_i} \sqrt{\left(\frac{P_s}{P_{si}} \frac{(P_T - P_s)}{h_i} \frac{T_{Ti}}{T_T} \right)} \right] \frac{2r\delta r}{R_2^2} \right\} \qquad \text{(II.20)}$$

In the mainstream, the term in square brackets, [ ], is very small, typically = 0·001. Therefore an error in the slide rule of (say) 0·1 per cent will produce an error in C_D of about 0·0001 per cent only. Had the same slide rule been used on equation (II.19) the resulting error in C_D would have been about 0·1 per cent. In the boundary layer, there is less to choose between equations (II.19) and (II.20) but since only about 12 per cent of the total flow is involved the slide rule is probably adequate for either equations (II.19) or (II.20). When using equation (II.19), even with a calculating machine, a check should be made that the values taken for r and δr satisfy

$$\frac{2}{R_2^2} \int r\,\delta r = 1{\cdot}0000$$

Alternatively, the factor $2r\,\delta r$ may be replaced by $\delta(r^2)$, which automatically sums correctly.

APPENDIX III

The Calculation of the Discharge Coefficient from Boundary-Layer Theory

As in Appendix II, the discharge coefficient is defined as the ratio of the true mass-flow rate to the indicated mass-flow rate. Thus, as in equation (II.1):

$$C_D = \frac{W_{\text{true}}}{W_i}.$$

In Appendix II, W_{true} was derived from local values of (ρu) obtained by traversing the nozzle, i.e. as in equation (II.2):

$$W_{\text{true}} = \int_A dW$$

or

$$W_{\text{true}} = \int_A \rho u \, dA \tag{III.1}$$

where A is the complete actual flow area in the traverse plane.

The present nozzle has been designed to generate a uniform ideal flow in the mainstream at the measuring plane. Consequently it is only in the thin boundary layer that the flow defects exist. It will be convenient to replace the actual area, A, by a smaller effective area, A', through which a uniform flow profile at the indicated mainstream level would pass to give the same true flow rate as equation (III.1). Thus:

$$\begin{aligned} W_{\text{true}} &= \int_{A'} (\rho u)_i \, dA \\ &= (\rho u)_i A'. \end{aligned} \tag{III.2}$$

Again, we have for the indicated flow rate:

$$W_i = (\rho u)_i A \tag{III.3}$$

therefore from equations (II.1), (III.2) and (III.3):

$$C_D = \frac{A'}{A}. \tag{III.4}$$

The reduction in the effective flow area from A to A' is caused by the boundary-layer displacement thickness, δ^*. The effective duct diameter becomes:

$$D' = D - 2\delta^* \tag{III.5}$$

where D is the actual diameter in the traverse plane. Hence we have for C_D:

$$\begin{aligned} C_D &= \frac{A'}{A} \\ &= \frac{(D-2\delta^*)^2}{D^2} \\ &= 1 - \frac{4\delta^*}{D} \end{aligned} \tag{III.6}$$

to a first order in δ^*/D.

The problem of evaluating δ^* over a range of mass-flow rates may be solved as follows:

(i) *Simplified theory for* δ^*.

In a simplified theory it would be assumed that there is no boundary-layer growth upstream of the first transition groove, and that δ^* is the value given by a turbulent boundary layer in a zero pressure gradient downstream of the first transition groove. Thus:

$$\delta^* = 0{\cdot}046x(R_x)^{-1/5} \tag{III.7}$$

where

$$R_x = \frac{\rho U x}{\mu} \tag{III.8}$$

$$= \frac{Wx}{A\mu} \tag{III.9}$$

and x is the length from the first transition groove to the traverse plane.

C_D could be calculated from equations (III.6), (III.7) and (III.9) over a range of W. In Fig. 16 these results are not shown; for clarity only the results obtained from the more refined theory given in (ii), below, have been shown.

(ii) *Refined theory for* δ^*.

It will be helpful to refer to Fig. 17. We assume a laminar boundary layer up to the first transition groove and a turbulent boundary layer thereafter, both occurring in a 'favourable' pressure gradient. It is convenient to replace the real nozzle and its two types of boundary layer by the equivalent parallel duct containing a turbulent boundary layer in a zero pressure gradient, as shown in Fig. 17. The displacement thickness is then given by:

$$\delta^* = 0{\cdot}046X_2(R_{X_2})^{-1/5} \tag{III.10}$$

for incompressible flow, or:

$$\delta^* = 0{\cdot}046\,(1+0{\cdot}8M^2)^{0{\cdot}44}X_2(R_{X_2})^{-1/5} \tag{III.11}$$

for compressible flow[22], i.e.

$$\frac{(\text{compressible } \delta^*)}{(\text{incompressible } \delta^*)} = (1+0{\cdot}8M^2)^{0{\cdot}44} \tag{III.12}$$

where X_2 is the equivalent parallel duct length.

An equation for X_2 is given in Ref. 20 as:

$$X_2 = 38{\cdot}2\left(\frac{\nu}{U_t}\right)^{3/8}\left(\frac{U_2}{U_t}\right)^{1/8}\left[\int_0^{x_t}\left(\frac{U}{U_2}\right)^5 dx\right]^{5/8} + \\ + \int_{x_t}^{x_2}\left(\frac{U}{U_2}\right)^3 dx \tag{III.13}$$

the notation in equation (III.13) being that of Ref. 22 rather than that of Ref. 20. The first term in equation (III.13) is the contribution of the laminar boundary layer. The second term is the contribution of the turbulent boundary layer in the real pressure gradient to give an effective turbulent length in a zero pressure gradient. Equation (III.13) is strictly for incompressible flow only, but for the low subsonic Mach numbers of the present type of nozzle the effect of

compressibility on the value of X_2 is very small[22]. Also equation (III.13) is based on the integrand $(U/U_2)^3$ for the turbulent boundary layer, whereas $(U/U_2)^4$ is now considered more accurate[22]. The effect on the present calculation is negligible, as the favourable gradient is small.

The integration in equation (III.13) need only be carried out once for a given nozzle, using one-dimensional theory to give:

$$\left(\frac{U}{U_2}\right) = \frac{A_2}{A}. \tag{III.14}$$

The integrations (which can conveniently be carried out graphically) yield the following constants for the present nozzle:

$$\int_0^{x_t} \left(\frac{U}{U_2}\right)^5 dx = 0{\cdot}04867 \text{ ft} \tag{III.15}$$

and

$$\int_{x_t}^{x_2} \left(\frac{U}{U_2}\right)^3 dx = 0{\cdot}860 \text{ ft}. \tag{III.16}$$

Again,

$$\left(\frac{\nu}{U_t}\right)^{3/8} = \left(\frac{\mu}{\rho U_t}\right)^{3/8}$$

$$= \left(\frac{\mu A_t}{W}\right)^{3/8}$$

$$= 1{\cdot}004 \times 10^{-2} \times W^{-3/8}. \tag{III.17}$$

(evaluating μ at 18°C).
Also,

$$\left(\frac{U_2}{U_t}\right)^{1/8} = \left(\frac{A_t}{A_2}\right)^{1/8}$$

$$= 1{\cdot}030. \tag{III.18}$$

Therefore from equations (III.13), (III.15), (III.16), (III.17) and (III.18):

$$X_2 = 38{\cdot}2 \times 1{\cdot}004 \times 10^{-2} \times W^{-3/8} \times 1{\cdot}030 \times (0{\cdot}04867)^{5/8} + 0{\cdot}860$$

$$= 5{\cdot}935 \times 10^{-2} \times W^{-3/8} + 0{\cdot}860. \tag{III.19}$$

C_D for incompressible flow can be calculated from equations (III.6), (III.10) and (III.19) over a range of W. It is shown as Curve (*b*) in Fig. 16.

For compressible flow the single curve of discharge coefficient against Reynolds number would in general be replaced by a family of curves, according to Mach number or pressure level. In the present tests all the traverses were made with approximately atmospheric static pressure in the measuring section, so that there is a one-to-one relationship in these tests between Reynolds number and Mach number. In fact the Mach number increases from about 0·25 when the Reynolds number is 10^6 and the mass flow is 6 lb/sec, to about 0·6 when the Reynolds number is 3×10^6 and the mass flow is 18 lb/sec. Correcting the incompressible results for these particular Mach numbers by way of equation (III.12) gives Curve (*c*) in Fig. 16.

For very low flow rates, when a laminar boundary layer would exist in the nozzle all the way to the traverse plane, a calculation similar to that for the incompressible turbulent boundary layer can be made using Thwaites' equation for the equivalent parallel duct length, viz:

$$X_2 = \int_0^{x_2} \left(\frac{U}{U_2}\right)^5 dx. \tag{III.20}$$

The value of δ^* is then given by:

$$\delta^* = 1{\cdot}72X_2(R_{X_2})^{-1/2}. \tag{III.21}$$

For the present nozzle, integration of equation (III.20) yields the value:

$$X_2 = 0{\cdot}8613 \text{ ft.} \tag{III.22}$$

C_D can be calculated from equations (III.6), (III.21) and (III.22) over a range of W. It is shown as Curve (*a*) in Fig. 16. Compressibility effects on C_D are negligible in the present nozzle in the laminar régime as the Mach numbers in that régime are very low.

APPENDIX IV

The Accuracy of the Discharge Coefficient

In the following paragraphs, random errors will be calculated at the 95 per cent confidence level. The relationship between random error, E, and standard deviation, σ, is:

$$E = t \times \sigma$$

The 95 per cent confidence value of 't' is 1·96 for large samples, but is somewhat greater for small samples. The actual value of 't' will be obtained from statistical tables for the appropriate number of independent observations (degrees of freedom) of the data.

1. *Components of Error.*

1.1. *Nozzle Wall Static Pressure, Random Error.*

A determination of static pressure is made by taking the mean reading of three or four different 0·063 in. wall statics and applying Shaw's correction for hole size. Thus we need to make allowance for not only the random error of the pressure readings, but also for any lack of a precise fit of Shaw's curve to our experimental results. This combined information is provided by the standard deviation of the points about the curve of Fig. 6, $\sigma(\Delta p)/\tau_w = 0{\cdot}170$,

therefore

$$\begin{aligned}\frac{\sigma(P_{si})}{h_i} &= \frac{\sigma(\Delta p)}{h_i} \\ &= \frac{\tau_w}{h_i}\frac{\sigma(\Delta p)}{\tau_w} \\ &= 0{\cdot}0035 \times 0{\cdot}170 \\ &= 0{\cdot}000595\end{aligned}$$

taking the ratio $\tau_w/h = 0{\cdot}0035$ from the table in Fig. 6 as typical of the whole range of dynamic pressures from $h = 6$ to $h = 170$ in. of water,

therefore

$$\begin{aligned}\frac{E(P_{si})}{h_i} &= \pm\, t \times \sigma \\ &= \pm\, 2{\cdot}06 \times 0{\cdot}000595 \\ &= \pm\, 0{\cdot}00122.\end{aligned}$$

An interesting point arises here. We have by definition:

$$C_D = \frac{\text{(true mass flow measured by traverse instrumentation)}}{\text{(indicated mass flow measured by fixed instrumentation)}}.$$

Since the corrected wall static gives both the 'traverse value' as well as the 'fixed indicated value', it follows that the error will have no apparent influence upon the numerical value of C_D. However, when the time comes to use the nozzle to calibrate another flowmeter the error of the static pressure must be taken into account for we then will have:

$$\text{(true mass flow)} = C_D \times \text{(indicated mass flow measured by fixed instrumentation)}$$

and it is the error of the right-hand side of this equation which we will need to know.

Now the equation for mass flow is:

$$W = k\sqrt{(h \times P_{si})}, \text{ approximately}$$

therefore

$$\frac{E(W)}{W_i} = \sqrt{\left\{\left(\tfrac{1}{2}\frac{E(h)}{h_i}\right)^2 + \left(\tfrac{1}{2}\frac{E(P_{si})}{P_{si}}\right)^2\right\}}.$$

The first term on the right-hand side $= \left(-\tfrac{1}{2}\dfrac{E(P_{si})}{h_i}\right)^2$

since

$$h = (P_T - P_s).$$

The second term can be neglected in comparison with the first term, since $P_{si} \gg h_i$. Thus we have:

$$\frac{E(W)}{W_i} = \pm\tfrac{1}{2} \times \frac{E(P_{si})}{h_i}$$

$$= \pm 0{\cdot}00061.$$

1.2. *Inlet static pressure.*

In practice there is only negligible scatter between the individual wall statics at nozzle inlet, and because of the low velocities there is no reason to expect any significant effect of finite hole size, nor of blemishes or dirt. Hence, any error in this measurement is negligible.

1.3. *Boundary-layer profiles.*

The scatter of the readings of the 18 wall-contact pitots will give a good estimate of the random error due to:

(*a*) Circumferential variation of the profile.

(*b*) Differences between individual pitots.

(*c*) Settings at wall-contact.

(*d*) Different tests.

In Section 4.5 we have justified the application of wall-contact data to within the boundary layer. We thus have a standard deviation within the boundary layer due to these causes of $\sigma(h)/h_i = 0{\cdot}0145$ for $h_i \simeq 50$ in. of water (*see* Section 4.5). This would give the random error of a single traverse. But we have improved the accuracy by making four separate traverses with the probe at 3, 6, 9 and 12 o'clock respectively to give the mean C_D of Fig. 15. Unfortunately, this involves only one probe and we would not be justified in asserting that $\sigma(\text{mean}) = \sigma/\sqrt{4}$. We know from Section 4.4 that about half of the overall variance is due to item (*a*) above, therefore we will use the compromise:

$$\sigma(\text{mean}) = \tfrac{3}{4}\sigma = 0{\cdot}0109$$

therefore

$$\frac{E(\text{mean } h)}{h_i} = t \times \sigma(\text{mean})$$

$$= 2{\cdot}11 \times 0{\cdot}0109$$

$$= 0{\cdot}0230$$

therefore in the boundary layer

$$\frac{E(\text{mean } W)}{W_i} = \tfrac{1}{2}\frac{E(\text{mean } h)}{h_i}$$

$$= 0{\cdot}0115.$$

Now, since we are regarding the boundary-layer annulus at the traverse plane as being 0·250 in. thick in a 7·500 in. diameter duct,

$$\text{(boundary-layer flow area)} = 0{\cdot}1289 \times \text{(total flow area)}$$

and since the percentage mass flow in the boundary layer is only slightly less than the percentage flow area, it is adequate to put:

$$\frac{E(\text{mean } C_D)}{C_D} = 0{\cdot}1285 \times \frac{E(\text{mean } W)}{W_i}$$
$$= 0{\cdot}00148.$$

1.4. *Size of Pitot Tubes in the Boundary Layer.*

In Section 4.6 we justified the limits of error $E(\epsilon)/D = \pm 0{\cdot}05$ for $h_i \simeq 50$ in. of water. When applied to a pitot of size $D = 0{\cdot}75$ mm, we have:

$$E(\epsilon) = \pm 0{\cdot}00145 \text{ in.}$$

but since

$$y_e = y_a + \epsilon:$$

therefore

$$E(y_e) = E(\epsilon).$$

It can be shown that an error in y_e of this magnitude is equivalent to an error in C_D of:

$$\frac{E(C_D)}{C_D} = \pm 0{\cdot}00040$$

1.5. *Bending of the Boundary-Layer Probe.*

The new 3 in. long boundary-layer probe of Fig. 4 was much stiffer than the old 10 in. probe of Fig. 3, but since any variation in tip deflection during a traverse has such a critical effect on accuracy it was necessary to check the deflection carefully. Unfortunately there was no obvious direct way of measuring deflections during an actual traverse and so an indirect method had to be used.

The two main modes of deflection are:

(*a*) Bending of the probe away from the wall due to flexing in the stem.

(*b*) Bending of the forward part of the probe towards the wall due to the couple exerted by the drag on the swan-neck tip.

Measurements of mode (*a*) deflections were made by loading the stem with weights on the bench. It was found that the change in deflection equivalent to traversing the probe across the boundary layer for $h_i \simeq 50$ in. of water was less than 0·0007 in. at the tip.

Measurements of mode (*b*) deflection were made by operating the probe in the nozzle at wall-contact with varying loading of dynamic pressure, using the electric wall-contact signal. The mode (*a*) flexing of the stem was not completely absent in this phase of the tests, but this flexing would be much less than that already studied during the weight loading tests on the bench. It was found that the change in mode (*b*) deflection, that would result from a traverse across the boundary layer at $h_i = 50$ in. of water, would be only 0·0001 in. at the tip.

Thus the combined change in tip deflection as the probe is traversed across the boundary layer at $h_i = 50$ in. of water would be less than 0·0006 in. It can be shown that the equivalent error in C_D is extremely small and is roughly given by $E(C_D)/C_D = 0{\cdot}00007$. This proportional error is itself directly proportional to h_i, but since it is such a small component of the total error its variation has been neglected in the analysis of accuracy.

1.6. *Mainstream Pitot-Pressure Traverses.*

The area-weighted mean 'circumferential' range of $(P_T - P_{Ti})/h_i$ in Fig. 15 is 0·000544, for $h_i \simeq 50$ in. of water. The corresponding standard deviation, from quality control tables for samples of $n = 4$, is:

$$\frac{\sigma(P_T)}{h_i} = 0{\cdot}000268$$

therefore

$$\frac{\sigma(\text{mean } P_T)}{h_i} = \frac{\sigma}{\sqrt{4}} = 0{\cdot}000134.$$

This implies a neglect of any error due to differences between individual pitots in the mainstream, in accordance with experience.

Therefore

$$\begin{aligned}\frac{E(\text{mean } P_T)}{h_i} &= \pm t \times \frac{\sigma(\text{mean } P_T)}{h_i} \\ &\simeq \pm 3{\cdot}18 \times 0{\cdot}000134 \\ &= \pm 0{\cdot}000426.\end{aligned}$$

Therefore in the mainstream:

$$\begin{aligned}\frac{E(\text{mean } W)}{W_i} &= \tfrac{1}{2}\frac{E(\text{mean } h)}{h_i} \\ &= \tfrac{1}{2}\frac{E(\text{mean } P_T)}{h_i}, \text{ since } h = P_T - P_s \\ &= \pm 0{\cdot}000213.\end{aligned}$$

Since the mainstream occupies 0·8715 of the total nozzle flow area, we have:

$$\begin{aligned}\frac{E(\text{mean } C_D)}{C_D} &= 0{\cdot}8715 \times \frac{E(\text{mean } W \text{ in mainstream})}{h_i} \\ &= \pm 0{\cdot}000186\end{aligned}$$

1.7. *Mainstream Static-Pressure Traverses.*

For convenience in analysing the static-pressure traverse results, we have asserted that the edge of the mainstream is at a nozzle radius of $r = 3{\cdot}5$ in., i.e. 0·250 in. from the wall. There is some uncertainty as to the exact position but it must surely be between $r = 3{\cdot}0$ in. and $r = 3{\cdot}5$ in., as a glance at the pitot-pressure profiles in the upper part of Fig. 15 will show. The worst possible error in $(P_s - P_{s,\,\text{edge}})/h_i$ that could possibly be introduced by the above simplification would be less than 0·0004 for the traverse from 6 to 12 o'clock, and less than 0·0001 for the mean of the four traverses. This latter value is equivalent to an error of about 0·00005 in C_D and has been neglected.

The area-weighted mean 'circumferential' range of $(P_s - P_{s,\text{edge}})/h_i$ in Fig. 15 is 0·000389 for $h_i \simeq 50$ in. of water. The corresponding standard deviation, from quality control tables for samples of $n = 4$, is:

$$\frac{\sigma(P_s)}{h_i} = 0{\cdot}000188$$

therefore

$$\frac{\sigma(\text{mean } P_s)}{h_i} = \frac{\sigma}{\sqrt{4}} = 0{\cdot}000094.$$

The error due to a foible of an individual static probe is eliminated by the artifice of equating the probe reading at the edge of the mainstream, $P_{s,\text{edge}}$, to the corrected average wall static pressure, P_{si} therefore

$$\begin{aligned}\frac{E(\text{mean } P_s)}{h_i} &= \pm t \times \frac{\sigma(\text{mean } P_s)}{h_i} \\ &= \pm 3{\cdot}18 \times 0{\cdot}000094 \\ &= \pm 0{\cdot}000299.\end{aligned}$$

By similar reasoning to that of Section 1.1:

$$\frac{E(\text{mean } W)}{W_i} = \tfrac{1}{2}\frac{E(\text{mean } P_s)}{h_i}.$$

Therefore in the mainstream:

$$\frac{E(\text{mean } W)}{W_i} = \pm 0{\cdot}000150.$$

Since the mainstream occupies 0·8715 of the total nozzle flow area, we have:

$$\begin{aligned}\frac{E(\text{mean } C_D)}{C_D} &= 0{\cdot}8715 \times \frac{E(\text{mean } W \text{ in mainstream})}{h_i} \\ &= \pm 0{\cdot}000131.\end{aligned}$$

1.8. *Air Temperature Traverses.*

The standard deviation of the traverse mean temperature is given in Section 5.3 as σ(traverse mean T) = 0·0646°C for $h_i \simeq 50$ in. of water. For an absolute temperature of $T = 300$°K, say, we have:

$$\frac{\sigma(\text{traverse mean } T)}{T} = 0{\cdot}000215$$

therefore

$$\begin{aligned}\frac{E(\text{traverse mean } T)}{T} &= \pm t \times \sigma \\ &= \pm 2{\cdot}57 \times 0{\cdot}000215 \\ &= \pm 0{\cdot}00055\end{aligned}$$

therefore

$$\begin{aligned}\frac{E(C_D)}{C_D} &= \frac{E(W)}{W} \\ &= \tfrac{1}{2}\frac{E(\text{traverse mean } T)}{T} \\ &= \pm 0{\cdot}00028.\end{aligned}$$

1.9. *Air-Temperature Absolute Determination.*

An N.G.T.E. type sonic suction pyrometer has a quoted accuracy of $\pm 0{\cdot}5$ per cent of the difference between hot-junction and cold-junction temperature. Assuming a 50°C difference between junctions we arrive at an accuracy of $\pm 0{\cdot}25$°C for any one pyrometer. If a total of three pyrometers were used, for which provision is made, the accuracy would be improved by a factor of $\sqrt{3}$ to $\pm 0{\cdot}14$°C. In non-dimensional terms of an absolute temperature of 300°K, say, the accuracy would be:

$$\frac{E(T)}{T} = \pm 0{\cdot}00083 \text{ for a single pyrometer}$$

or

$$\frac{E(T)}{T} = \pm 0{\cdot}00048 \text{ for the mean of three pyrometers.}$$

This leans to an error in indicated mass flow of:

$$\frac{E(W_i)}{W_i} = \tfrac{1}{2} \times \frac{E(T)}{T}$$

$$= \pm 0{\cdot}00041 \text{ for one pyrometer}$$

or

$$= \pm 0{\cdot}00024 \text{ for the mean of three pyrometers.}$$

1.10. *Manometers.*

In general, pressure tappings have been connected to 5 mm precision-bore manometers which are backed off against a reference pressure of similar magnitude. The manometer errors of these small readings of $(P - P_{\text{ref}})$ are negligible (for example, *see* Table 1, Section 4.3).

The following measured quantities are of larger magnitude:

(*a*) Indicated dynamic pressure, h_i (Section 2.7).

(*b*) Absolute value of P_{si} (Section 2.7).

(*c*) Pitot traverses in the boundary layer (Sections 4.5, 4.6 and 5.1).

As mentioned in Section 2.6, the quantities (*a*) and (*b*) are measured on suitable manometers such as the type constructed from 1 in. diameter glass tubing which reduces the meniscus error. It is considered that the worst manometer error of any one individual reading (say $0{\cdot}01$ in. at $h = 10$ in. of water) would not exceed $0{\cdot}05$ per cent in terms of nozzle mass flow, and usually the error would be much less. Hence this component of error, which would apply to the measurement of the indicated airflow rate, has been neglected.

It has been found adequate to measure quantity (*c*) on ordinary 4 mm bore manometers. The meniscus errors involved are negligible compared with the general variability found in the boundary layer.

2. *Analysis of Overall Accuracy.*

2.1. *Accuracy of the Numerical Value of the Mean Traverse C_D.*

For reasons of economy, most of the random errors affecting the numerical value of the traverse C_D have only been determined at the single, typical, condition: $h_i \simeq 50$ in. of water, and are shown

in Table 2 below. It seems reasonable to expect only slight variation with h_i of these non-dimensional errors. An exception is that due to bending of the boundary-layer probe, but since it is such a small component its variation has been neglected (*see* Section 1.5).

TABLE 2

Section	Source of random error Title	Component of error $\frac{E(C_D)}{C_D}$ at 95 per cent confidence level	E^2
1.3	Boundary-layer profiles: (*a*) Circumferential variation (*b*) Differences between pitots (*c*) Setting at wall-contact (*d*) Between tests	0·00148	$219{\cdot}0 \times 10^{-8}$
1.4	Size of boundary-layer pitot tip	0·00040	$16{\cdot}0 \times 10^{-8}$
1.5	Bending of boundary-layer probe . . .	0·00007	$0{\cdot}5 \times 10^{-8}$
1.6	Mainstream pitot traverse	0·00019	$3{\cdot}6 \times 10^{-8}$
1.7	Mainstream static traverse	0·00013	$1{\cdot}7 \times 10^{-8}$
1.8	Air-temperature traverse	0·00028	$7{\cdot}9 \times 10^{-8}$
	Overall, $\sqrt{\{\sum(E^2)\}}$	0·00158	$248{\cdot}7 \times 10^{-8}$

2.2. *Accuracy of the Instrumentation for the Indicated Mass Flow.*

The errors of the instrumentation for the indicated mass-flow rate (rather than errors in the numerical value of C_D obtained by traverse) are given in the following Table 3. They apply over the whole operating range of the nozzle.

TABLE 3

Section	Source of random error Title	Component of error $\frac{E(W)}{W_i}$ at 95 per cent confidence level	E^2
1.2	Nozzle inlet static pressure	negligible	0
1.1	Traverse-plane static pressure	0·00061	$37{\cdot}2 \times 10^{-8}$
1.8	Air temperature	0·00024	$5{\cdot}8 \times 10^{-8}$
	Overall, $\sqrt{\{\sum(E^2)\}}$	0·00066	$43{\cdot}0 \times 10^{-8}$

2.3. *Accuracy of the Determination of True Mass-Flow Rate.*

The overall random error is the combined errors of the two factors in the right-hand side of the equation:

$$W_{\text{true}} = C_D \times W_i$$

therefore

$$\frac{E(W_{\text{true}})}{W_{\text{true}}} = \sqrt{\left[\frac{E(C_D)}{C_D}\right]^2 + \left[\frac{E(W_i)}{W_i}\right]^2}.$$

The combination is shown in the following table:

TABLE 4

Section	Source of random error Title	Component of error E at 95 per cent confidence level	E^2
2.1	Mean traverse C_D	0·00158	$248{\cdot}7 \times 10^{-8}$
2.2	Instrumentation for the indicated mass flow . .	0·00066	$43{\cdot}0 \times 10^{-8}$
	Overall, $\sqrt{\{\Sigma(E^2)\}}$	0·00171	$291{\cdot}7 \times 10^{-8}$

Thus the final estimate of the accuracy of measurement of true mass-flow rate is $\pm 0{\cdot}171$ per cent due to random error.

From Table 4 it can be seen that the error of the discharge coefficient (0·00158) dominates the error of the instrumentation for the indicated mass flow (0·00066). Table 2 shows that by far the biggest error component of the discharge coefficient is contained within the boundary layer (0·00148). The simple analysis of Section 4.3 indicates that the most important elements of error in the boundary layer are those due to (*a*) circumferential variations and (*b*) differences between individual pitots. It is felt that the element of error due to circumferential variation could be reduced with the manufacture of a new nozzle. If the elimination of error due to circumferential variation were to reduce the boundary-layer component from 0·00148 to 0·00070, say, this would reduce the overall error of C_D from 0·00158 to 0·00089 and reduce the overall error of true mass flow from 0·00171 to 0·00110.

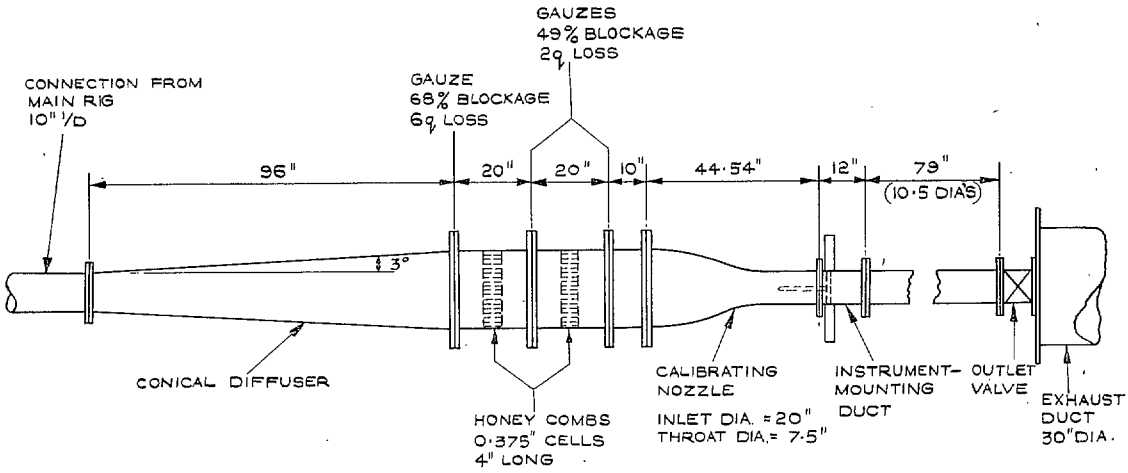

FIG. 1. Calibrating-nozzle ducting.

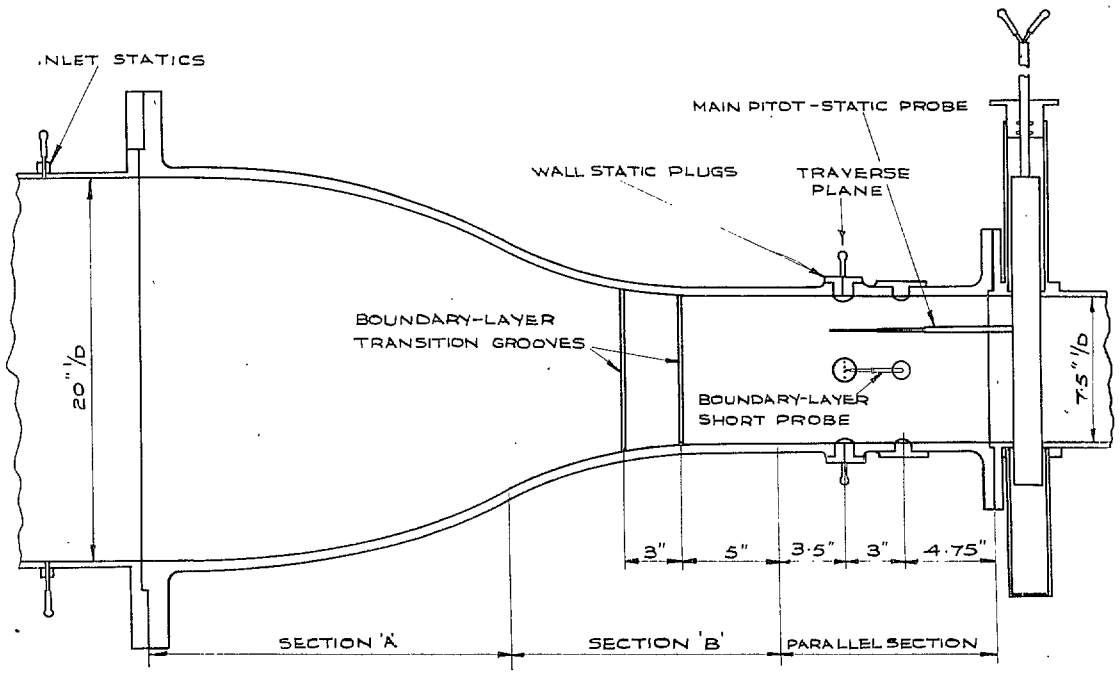

FIG. 2. Calibrating-nozzle assembly.

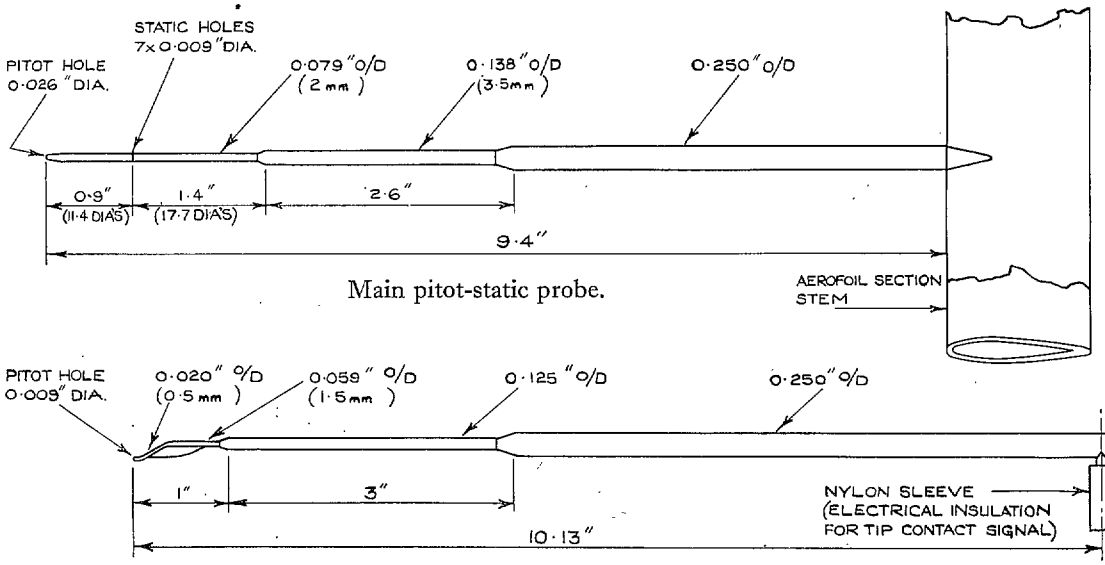

Main pitot-static probe.

Long boundary-layer pitot probe.

FIG. 3. Traversing instruments.

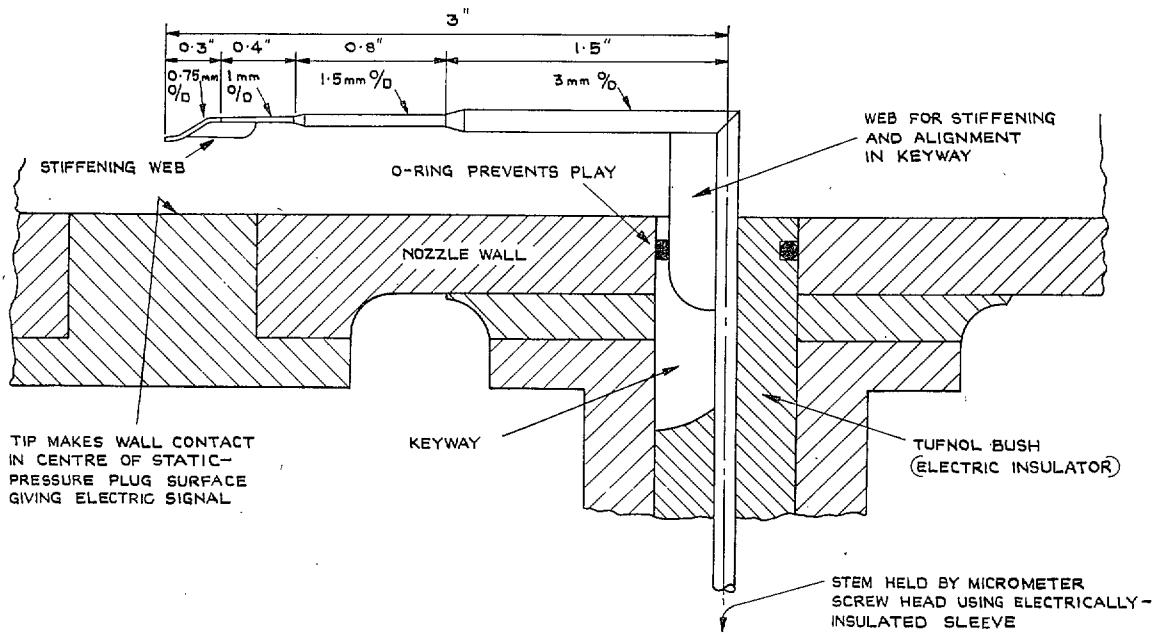

FIG. 4. Short boundary-layer probe.

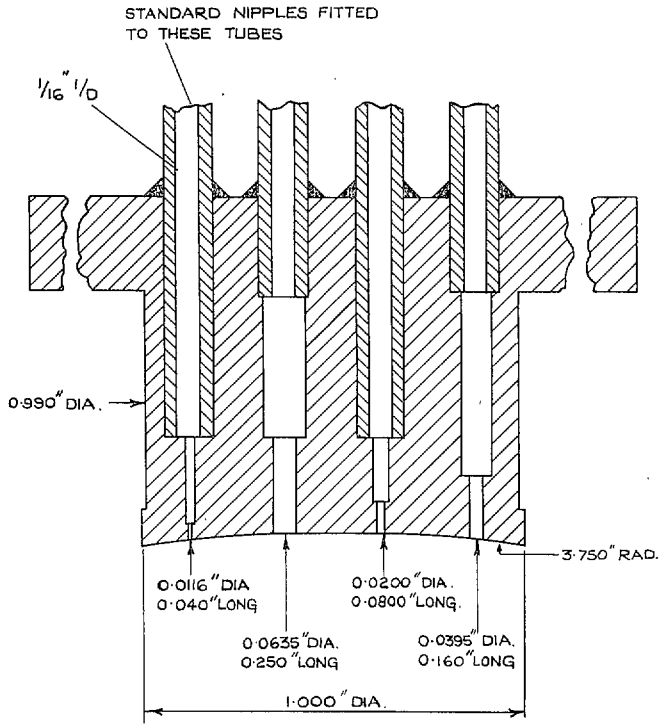

NOTE: ALL THE STATIC HOLES ARE 4 DIA'S LONG, THEN ENLARGE TO TWICE THE SURFACE DIA. BEFORE COMMUNICATING WITH 1/16" I/D TUBING.

FIG. 5. Wall static-pressure plug.

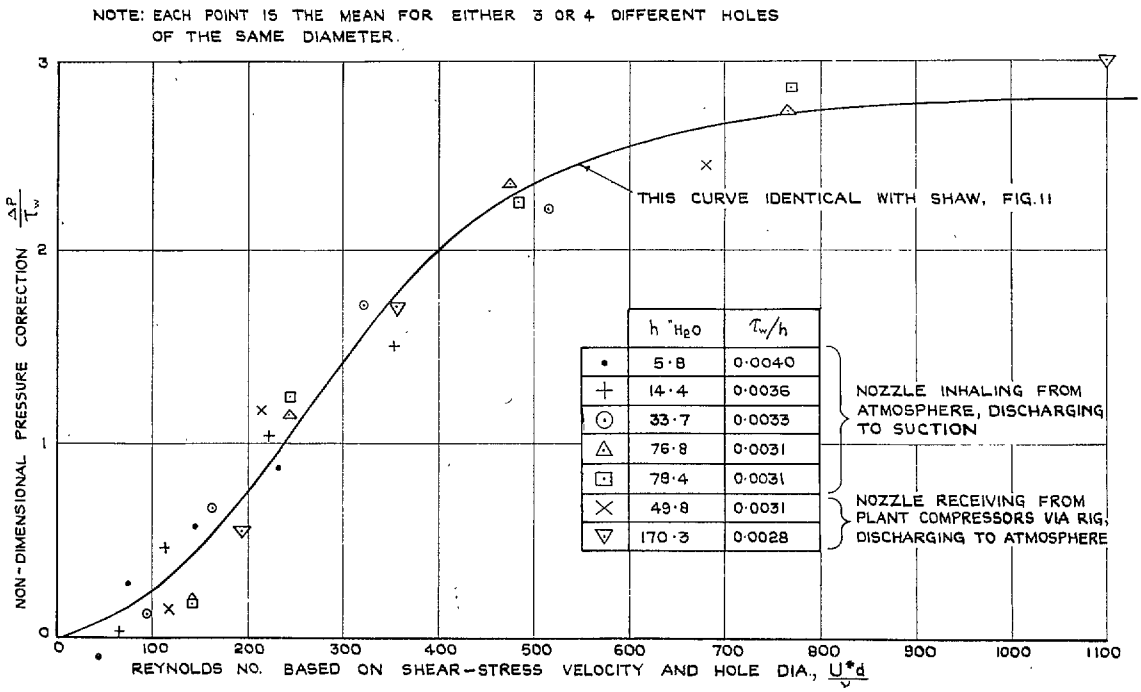

FIG. 6. Static-pressure correction due to hole size.

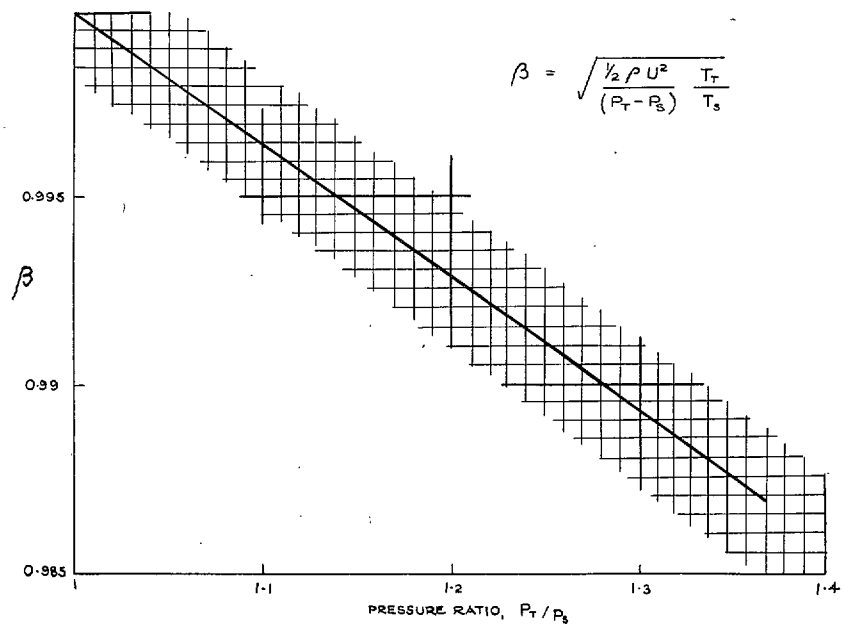

FIG. 7. Compressibility factor, β.

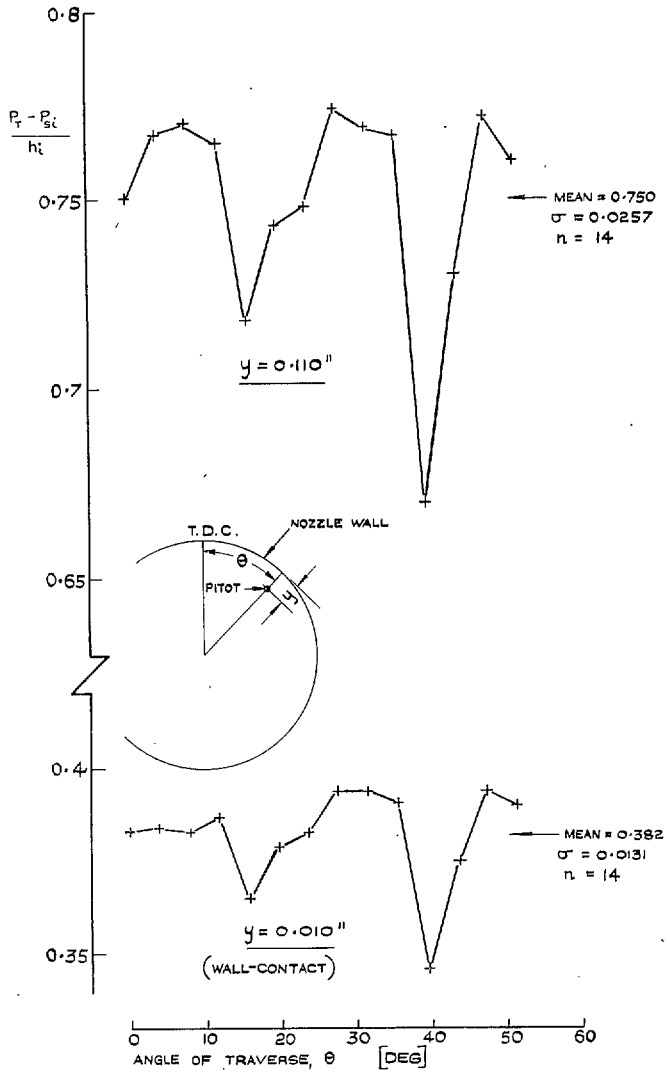

FIG. 8. Preliminary angular traverse of boundary layer. (10 in. long pitot probe, 0·5 mm tip.)

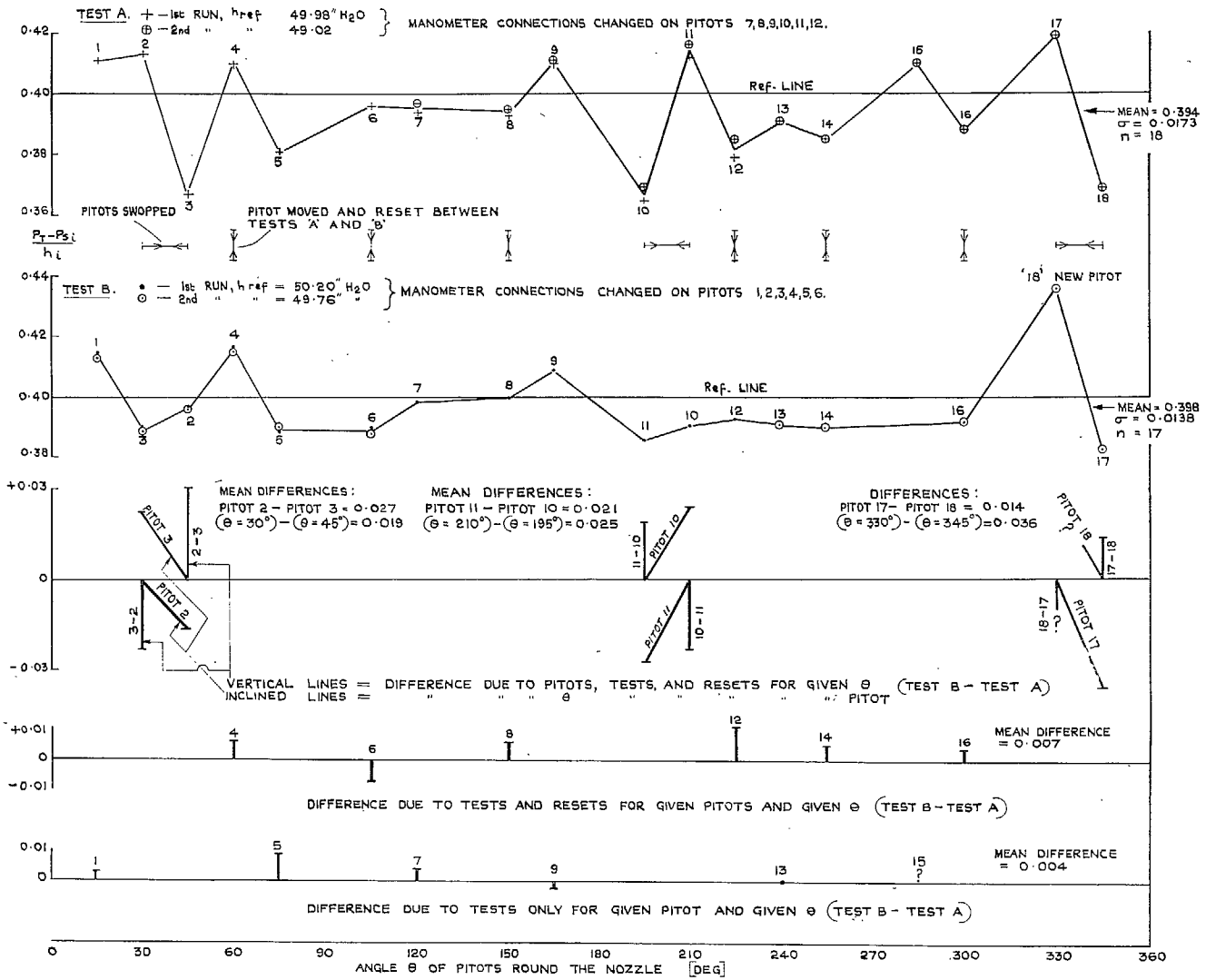

FIG. 9. The wall-contact pitots experiments.

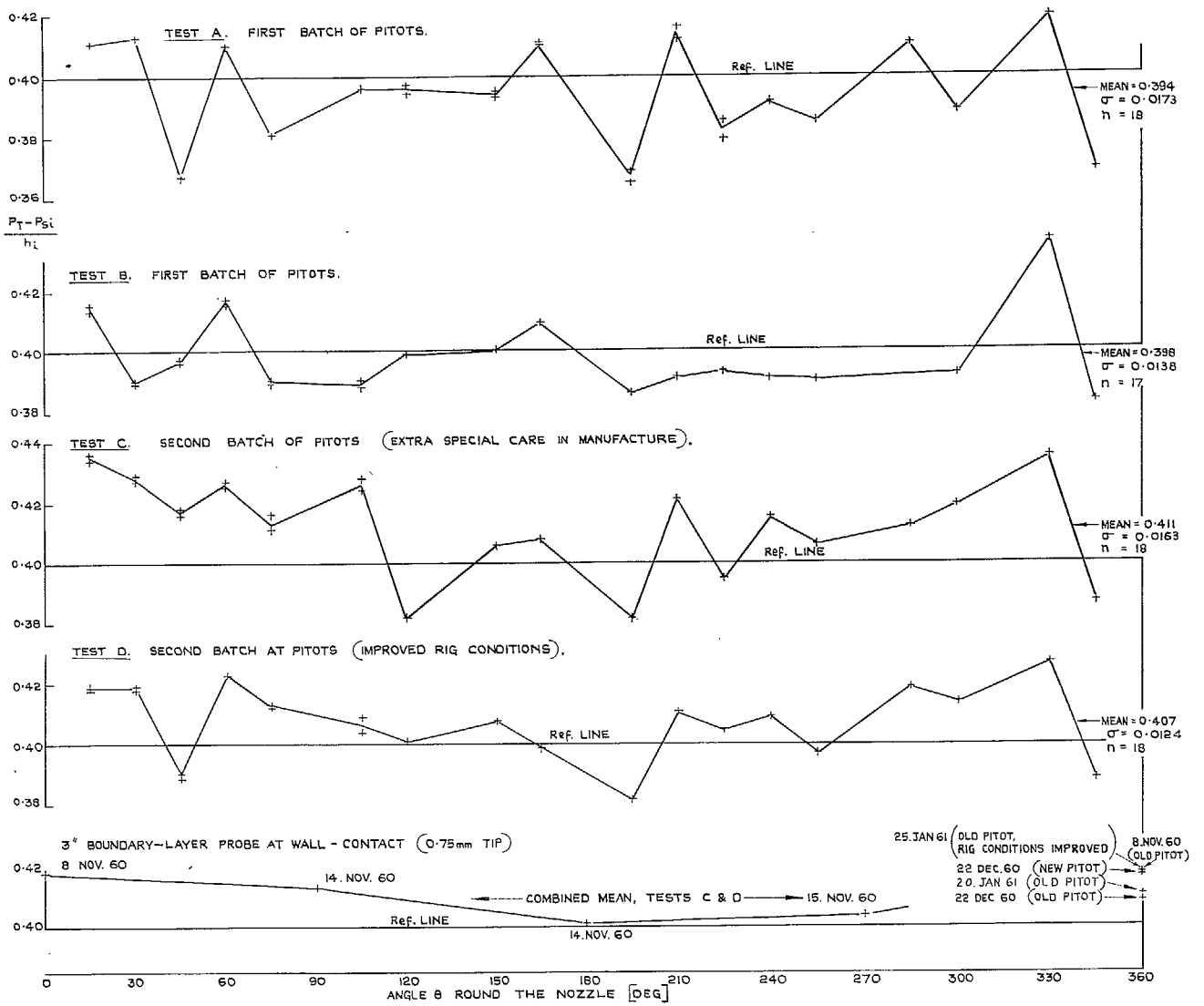

FIG. 10. Further comparison of wall-contact pitot results (0·75 mm tips).

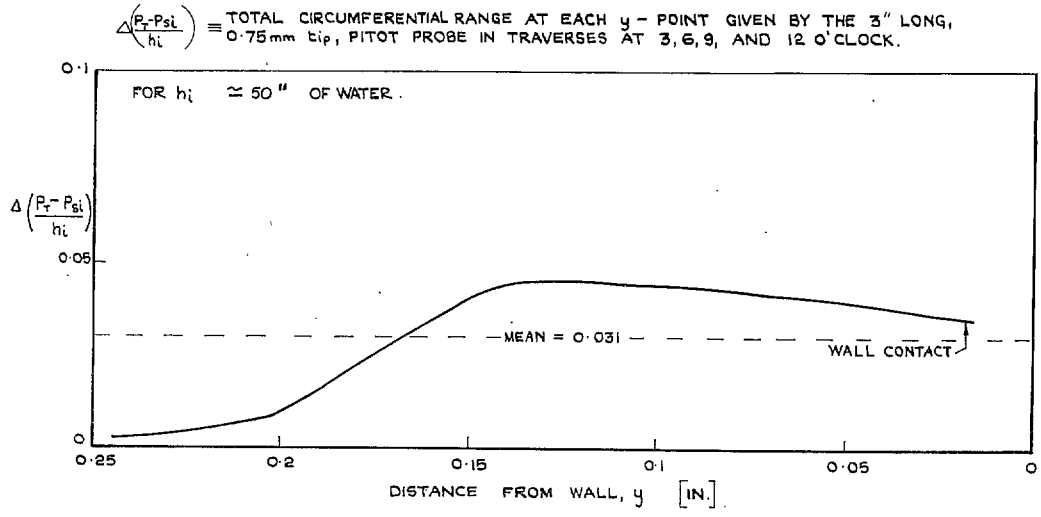

FIG. 11. Circumferential variation of dynamic pressure in boundary-layer traverses.

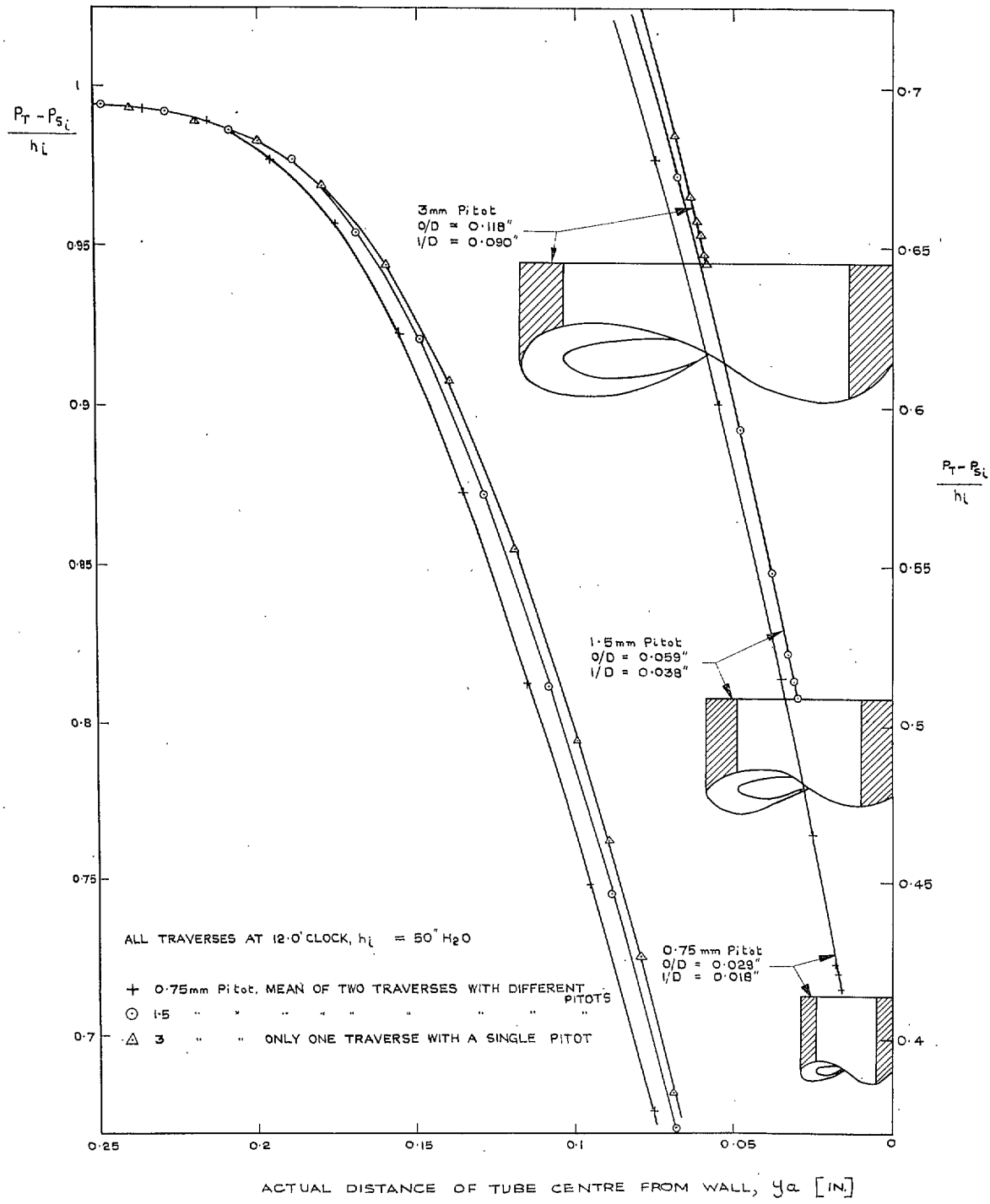

FIG. 12. Effect of pitot-tube size in boundary layer.

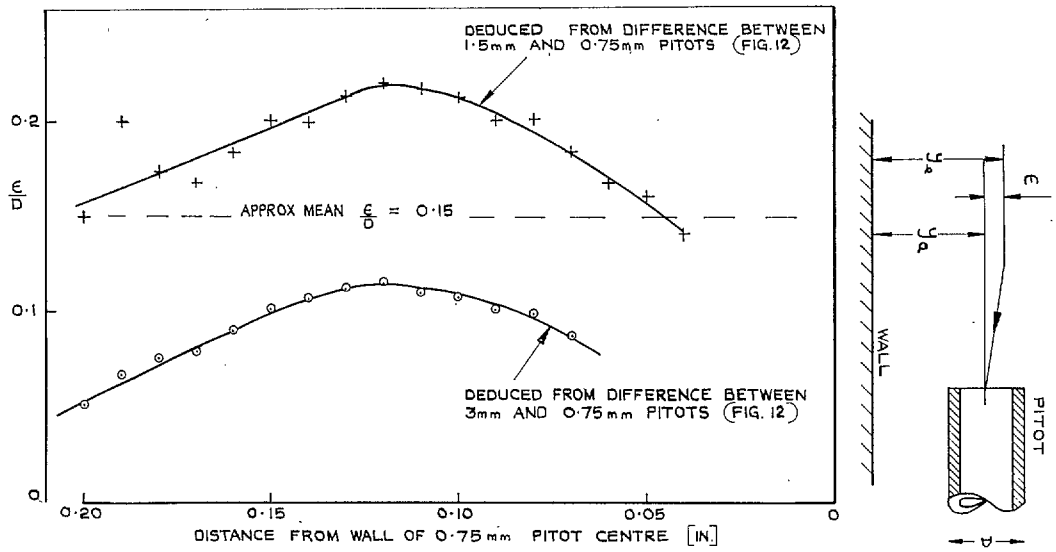

[FIG. 13. Effective displacement of pitot tubes in boundary layer.

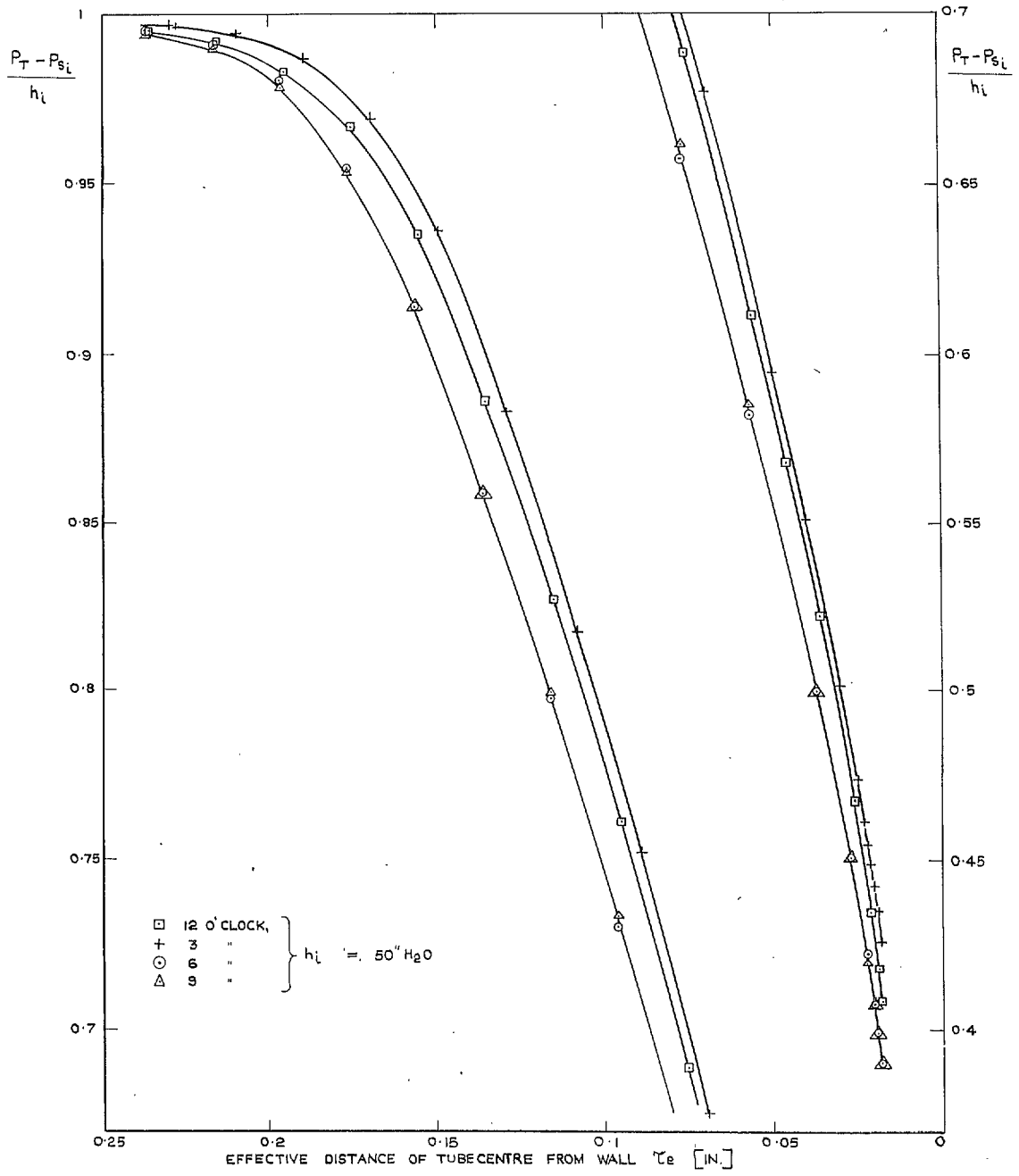

FIG. 14. Example of final boundary-layer traverses.

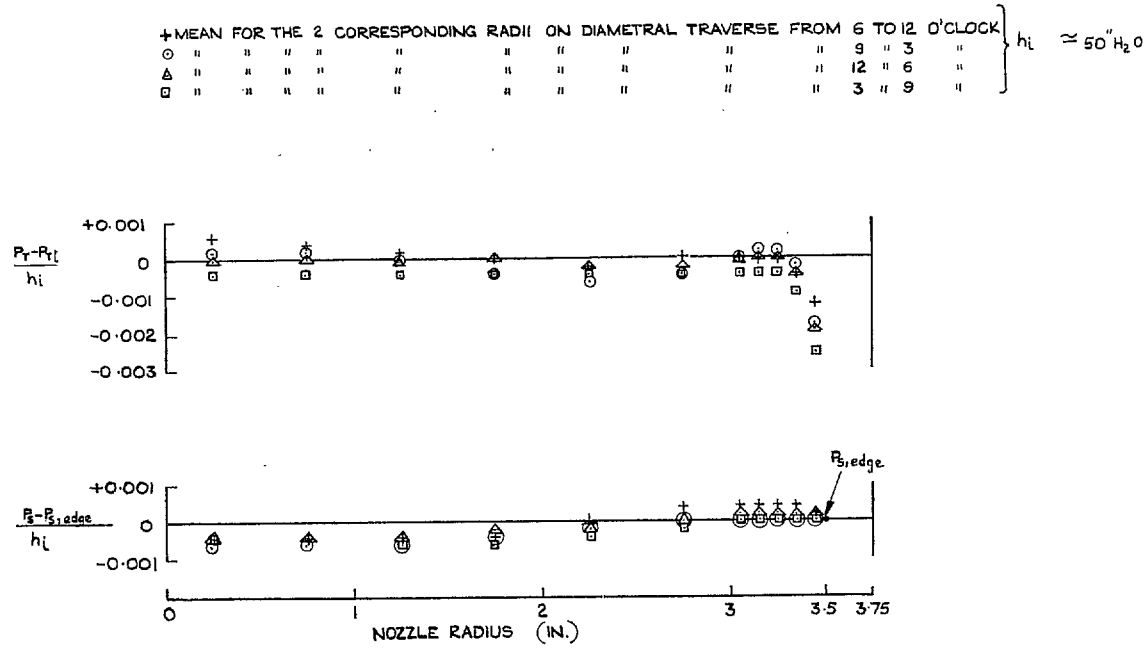

FIG. 15. Example of final mainstream traverse.

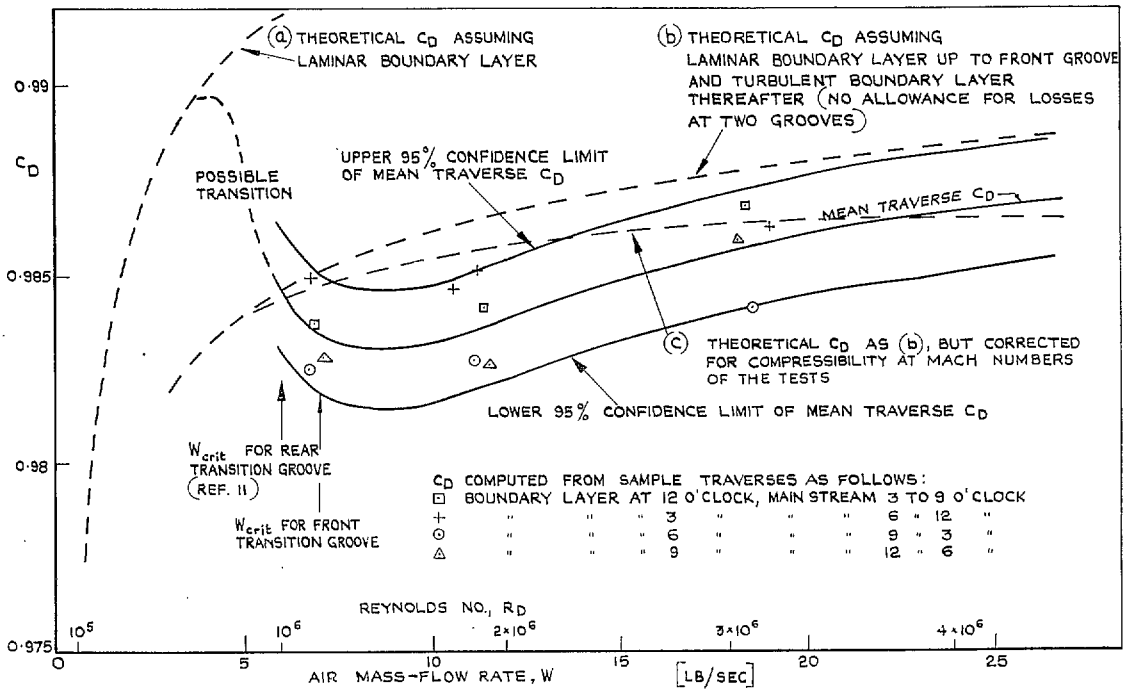

FIG. 16. The nozzle discharge coefficient.

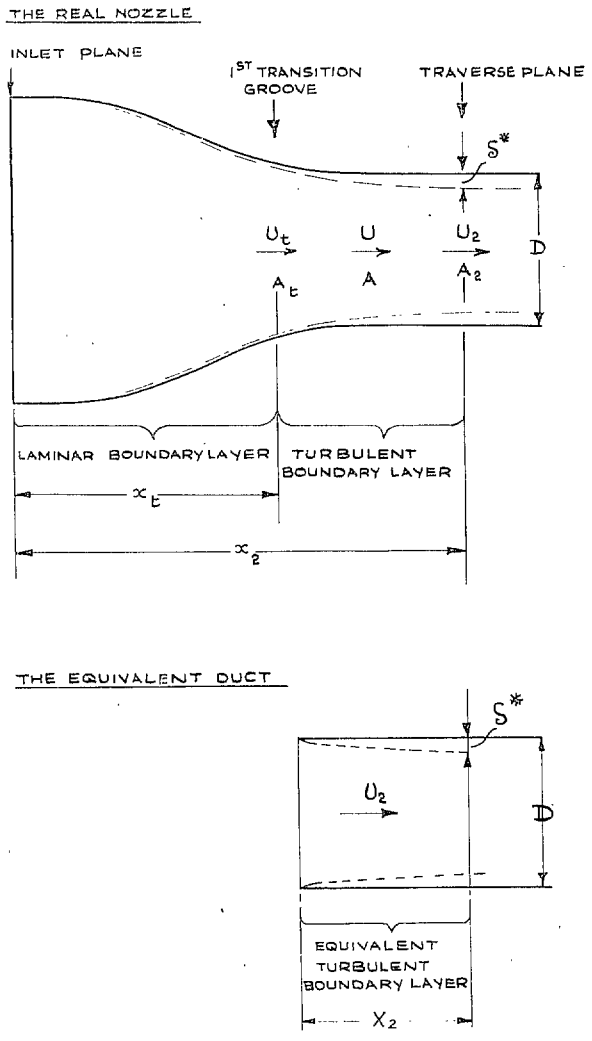

FIG. 17. The theoretical boundary-layer displacement thickness (*see* Appendix III).

(90227) Wt. 66/2301 K.5 10/64 Hw.

Publications of the Aeronautical Research Council

ANNUAL TECHNICAL REPORTS OF THE AERONAUTICAL RESEARCH COUNCIL (BOUND VOLUMES)

1942 Vol. I. Aero and Hydrodynamics, Aerofoils, Airscrews, Engines. 75*s.* (post 2*s.* 9*d.*)
Vol. II. Noise, Parachutes, Stability and Control, Structures, Vibration, Wind Tunnels. 47*s.* 6*d.* (post 2*s.* 3*d.*)

1943 Vol. I. Aerodynamics, Aerofoils, Airscrews. 80*s.* (post 2*s.* 6*d.*)
Vol. II. Engines, Flutter, Materials, Parachutes, Performance, Stability and Control, Structures. 90*s.* (post 2*s.* 9*d.*)

1944 Vol. I. Aero and Hydrodynamics, Aerofoils, Aircraft, Airscrews, Controls. 84*s.* (post 3*s.*)
Vol. II. Flutter and Vibration, Materials, Miscellaneous, Navigation, Parachutes, Performance, Plates and Panels, Stability, Structures, Test Equipment, Wind Tunnels. 84*s.* (post 3*s.*)

1945 Vol. I. Aero and Hydrodynamics, Aerofoils. 130*s.* (post 3*s.* 6*d.*)
Vol. II. Aircraft, Airscrews, Controls. 130*s.* (post 3*s.* 6*d.*)
Vol. III. Flutter and Vibration, Instruments, Miscellaneous, Parachutes, Plates and Panels, Propulsion. 130*s.* (post 3*s.* 3*d.*)
Vol. IV. Stability, Structures, Wind Tunnels, Wind Tunnel Technique. 130*s.* (post 3*s.* 3*d.*)

1946 Vol. I. Accidents, Aerodynamics, Aerofoils and Hydrofoils. 168*s.* (post 3*s.* 9*d.*)
Vol. II. Airscrews, Cabin Cooling, Chemical Hazards, Controls, Flames, Flutter, Helicopters, Instruments and Instrumentation, Interference, Jets, Miscellaneous, Parachutes. 168*s.* (post 3*s.* 3*d.*)
Vol. III. Performance, Propulsion, Seaplanes, Stability, Structures, Wind Tunnels. 168*s.* (post 3*s.* 6*d.*)

1947 Vol. I. Aerodynamics, Aerofoils, Aircraft. 168*s.* (post 3*s.* 9*d.*)
Vol. II. Airscrews and Rotors, Controls, Flutter, Materials, Miscellaneous, Parachutes, Propulsion, Seaplanes, Stability, Structures, Take-off and Landing. 168*s.* (post 3*s.* 9*d.*)

1948 Vol. I. Aerodynamics, Aerofoils, Aircraft, Airscrews, Controls, Flutter and Vibration, Helicopters, Instruments, Propulsion, Seaplane, Stability, Structures, Wind Tunnels. 130*s.* (post 3*s.* 3*d.*)
Vol. II. Aerodynamics, Aerofoils, Aircraft, Airscrews, Controls, Flutter and Vibration, Helicopters, Instruments, Propulsion, Seaplane, Stability, Structures, Wind Tunnels. 110*s.* (post 3*s.* 3*d.*)

Special Volumes

Vol. I. Aero and Hydrodynamics, Aerofoils, Controls, Flutter, Kites, Parachutes, Performance, Propulsion, Stability. 126*s.* (post 3*s.*)
Vol. II. Aero and Hydrodynamics, Aerofoils, Airscrews, Controls, Flutter, Materials, Miscellaneous, Parachutes, Propulsion, Stability, Structures. 147*s.* (post 3*s.*)
Vol. III. Aero and Hydrodynamics, Aerofoils, Airscrews, Controls, Flutter, Kites, Miscellaneous, Parachutes, Propulsion, Seaplanes, Stability, Structures, Test Equipment. 189*s.* (post 3*s.* 9*d.*)

Reviews of the Aeronautical Research Council

1939–48 3*s.* (post 6*d.*) 1949–54 5*s.* (post 5*d.*)

Index to all Reports and Memoranda published in the Annual Technical Reports

1909–1947 R. & M. 2600 (out of print)

Indexes to the Reports and Memoranda of the Aeronautical Research Council

Between Nos. 2351–2449	R. & M. No. 2450 2*s.* (post 3*d.*)
Between Nos. 2451–2549	R. & M. No. 2550 2*s.* 6*d.* (post 3*d.*)
Between Nos. 2551–2649	R. & M. No. 2650 2*s.* 6*d.* (post 3*d.*)
Between Nos. 2651–2749	R. & M. No. 2750 2*s.* 6*d.* (post 3*d.*)
Between Nos. 2751–2849	R. & M. No. 2850 2*s.* 6*d.* (post 3*d.*)
Between Nos. 2851–2949	R. & M. No. 2950 3*s.* (post 3*d.*)
Between Nos. 2951–3049	R. & M. No. 3050 3*s.* 6*d.* (post 3*d.*)
Between Nos. 3051–3149	R. & M. No. 3150 3*s.* 6*d.* (post 3*d.*)

HER MAJESTY'S STATIONERY OFFICE

from the addresses overleaf

Printed and published by
HER MAJESTY'S STATIONERY OFFICE

To be purchased from
York House, Kingsway, London W.C.2
423 Oxford Street, London W.1
13A Castle Street, Edinburgh 2
109 St. Mary Street, Cardiff
39 King Street, Manchester 2
50 Fairfax Street, Bristol 1
35 Smallbrook, Ringway, Birmingham 5
80 Chichester Street, Belfast 1
or through any bookseller

Printed in England

S.O. Code No. 23-3384